Master Thesis

July 4, 2025

# Computational investigation of pentalene dimerization and antiaromatic reactivity


**Carles Alcaide i Blaya**

**supervised by**

Prof. Dr. Miquel Solà i Puig

Dr. Sílvia Simon Rabaseda


Master in Advanced Catalysis
and Molecular Modelling (MACMOM)


Universitat de Girona
Facultat de Ciències

diMOcat

iQCC
Institut de Química
Computacional i Catàlisi

**Master Thesis**

**Computational investigation of pentalene dimerization and antiaromatic reactivity**

**Author:** Carles Alcaide i Blaya, carlesalcaideblaya@gmail.com

**Supervision:** Prof. Dr. Miquel Solà i Puig, miquel.sola@udg.edu

Dr. Sílvia Simon Rabaseda, silvia.simon@udg.edu

**Project period:** 02/04/2025 - 04/07/2025

Institut de Química Computacional i Catàlisi, DIMOCAT

Departament de Química, Universitat de Girona

Date of diposit of the report at the academic secretary office: 04/07/2025

# Abstract

Antiaromatic molecules are characterized by their electronic instability, leading to high reactivity and limited synthetic accessibility. Among these systems, pentalene serves as a prototypical antiaromatic hydrocarbon, whose chemical behavior is governed by its formal 8 $\pi$-electron configuration. This thesis presents a comprehensive computational study of the dimerization of pentalene and its derivatives, aiming to elucidate the thermodynamic and kinetic factors that govern their reactivity. Using density functional theory (DFT) at the B3LYP-GD3BJ/6-311++G** level of theory, I characterized the potential energy surfaces of unsubstituted and functionally substituted pentalenes, analyzing both transition states and product geometries. The study evaluates how steric and electronic effects—introduced via functional groups such as —OH, —CN, —COOMe, -–CHO, and —t-Bu, affect the activation barriers, reaction energies, HOMO–LUMO gaps, and aromaticity indices (MCI and $I_{ring}$). Particular attention is paid to the interplay between antiaromatic destabilization and substituent-induced modulation of dimerization propensity. The results reveal that bulky or electron-withdrawing substituents can significantly alter both the thermodynamic favorability and kinetic accessibility of the dimerization reaction. Key conceptual tools such as the Maximum Hardness Principle, the Global Electrophilicity Index, the Bell–Evans–Polanyi relationship, and the Hammond–Leffler postulate are applied to rationalize the observed reactivity trends. This work provides mechanistic insight and predictive guidelines for designing pentalene-based systems with tailored stability and reactivity, relevant for applications in materials science and organic electronics.

# Contents

# Chapter 1

# Introduction

## 1.1 Aromaticity and antiaromaticity in organic chemisry

Aromaticity — and its counterpart, antiaromaticity — are foundational concepts in organic chemistry, central to understanding the stability, reactivity, and electronic behavior of cyclic $\pi$-conjugated molecules.[1],[2],[3] These principles underpin the properties of countless organic compounds, from fundamental building blocks to complex natural products and advanced functional materials. The most well-established framework for classifying aromatic systems is Hückel's rule, developed from the foundational work of Doering and Detert,[4] which states that planar, monocyclic, fully conjugated systems containing (4n+2) $\pi$-electrons exhibit remarkable aromatic stability.[5] In stark contrast, systems with 4n $\pi$-electrons under the same geometric and electronic constraints are classified as antiaromatic. These are typically characterized by significant destabilization due to unfavorable electronic delocalization and disruptive orbital interactions, often leading to enhanced reactivity.[6]

The term "aromaticity" was first introduced in 1855,[7] originally coined to describe phenyl-type compounds that possessed noticeable aromas, in contrast to odorless saturated hydrocarbons. Although it was later discovered that these characteristic smells had no direct chemical connection to aromatic behavior or electronic delocalization, the name persisted as a designation for unique $\pi$-conjugated cyclic compounds. A pivotal moment in the structural understanding of aromaticity occurred in 1865, when August Kekulé proposed the hexatriene ring structure of benzene.

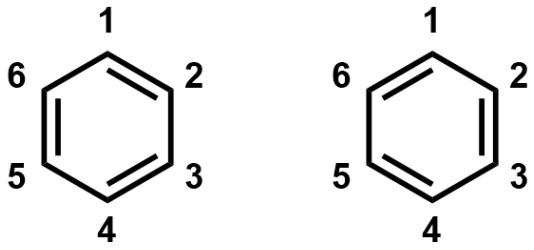


**Figure 1.1**: Kekulé structures of benzene.

This landmark proposal marked the beginning of the structural era of aromatic chemistry, emphasizing the cyclic arrangement of atoms. With the advent of quantum mechanics, a new conceptual framework emerged for interpreting molecular systems, providing a deeper understanding of electron distribution and bonding. This included the development of electron wavefunction theory, which allowed chemists to describe $\pi$-electron delocalization mathematically. Quantum mechanical models definitively confirmed that benzene consists of six carbon atoms arranged in a cyclic, planar geometry, with $\pi$-electrons delocalized evenly across the entire ring — an insight that laid the groundwork for modern theories of aromatic stabilization and orbital symmetry, moving beyond purely structural considerations to embrace electronic principles.

However, despite its pervasive use and predictive power, aromaticity remains a multifaceted concept without a strict, universally agreed-upon definition. As has been consistently emphasized in the literature, "*no single property exists that could be taken as a direct measure of aromaticity.*"[8] This inherent ambiguity has necessitated the development of diverse aromaticity descriptors, each probing a different aspect of this complex phenomenon. These descriptors are typically grouped into four main categories: energetic descriptors (indicating the aromatic stabilization energy), magnetic indicators (reflecting induced ring currents), geometric parameters (such as bond length alternation and planarity), and electronic delocalization-based indices (quantifying electron sharing and delocalization). Although aromaticity is not directly observable, it is inferred from a variety of experimental and computational criteria, including resonance energy[9], deviations from ideal bond length alternation, deviations from planarity[10], magnetic response (such as diatropic or paratropic induced ring currents), chemical shielding tensors (e.g., Nucleus-Independent Chemical Shift, NICS),[11],[12],[13] and electron delocalization indices.[14],[15] These robust tools allow researchers to qualitatively and quantitatively compare degrees of (anti)aromaticity across a vast array of molecular systems, provid-

ing a nuanced understanding of their electronic characteristics.

Antiaromatic molecules, in particular, display physical and spectroscopic features that contrast sharply with their aromatic analogs. These include the manifestation of paratropic ring currents,[16],[17] characteristically narrow HOMO – LUMO (Highest Occupied Molecular Orbital — Lowest Unoccupied Molecular Orbital) gaps,[18] and significantly increased chemical reactivity. This inherent electronic instability in antiaromatic systems can also be understood through the lens of the Maximum Hardness Principle (MHP).[19] According to the MHP, chemical systems tend to evolve towards states of maximal chemical hardness, where hardness ($\eta$) is directly related to the HOMO – LUMO energy gap and it is calculated as in Eq. 1.1

$$\eta = \frac{LUMO - HOMO}{2} \tag{1.1}$$

Antiaromatic compounds, characterized by their narrow HOMO – LUMO gaps, possess low chemical hardness, rendering them highly reactive as they strive to achieve a more stable, higher-hardness state, often through chemical transformations like dimerization. As a direct result of their inherent electronic strain, antiaromatic systems often seek to relieve their instability through various mechanisms. These commonly include facile dimerization reactions, non-planar distortions (puckering or twisting) that break conjugation, or redox transformations that alter the $\pi$-electron count and shift the aromatic character.[20] The concept of aromaticity has also been extended to excited-state systems, most notably through Baird's rule.[21] This model predicts that in the lowest triplet excited state ($T_1$), 4n $\pi$-electron systems become aromatic, while $(4n + 2)$ systems become antiaromatic.[22] This excited-state reversal, explained using both molecular orbital (MO) and valence bond (VB) theoretical models,[23] has profound implications for understanding photoreactivity and designing molecules for photoinduced electron transfer and optoelectronic applications.[24],[25],[26] More recently, researchers have introduced the concept of "concealed antiaromaticity",[27] which refers to systems that ingeniously hide their antiaromatic nature under ground-state conditions but reveal aromatic or antiaromatic behavior upon redox changes or photoexcitation. Structural motifs such as locally aromatic subunits sharing $\pi$-electrons with a 4n $\pi$-system, or intramolecular connections that disrupt planarity, are among the clever strategies employed to stabilize otherwise highly reactive antiaromatic frameworks. Despite the historical dominance of aromatic systems in chemical literature, antiaromatic compounds are currently gaining renewed attention—not only as intriguing reactive curiosities but also as highly promis-

ing functional materials with potential applications in organic electronics, photovoltaics, and molecular switches.[28],[29],[30],[31],[32],[33],[34],[35]Their tunable electronic properties, including low-lying triplet states and small HOMO–LUMO gaps, make them attractive candidates for integration into next-generation materials platforms.

## 1.2 Pentalene: a prototypical antiaromatic system

Among the structurally simplest and most emblematic antiaromatic systems is pentalene (Figure 1.2), a hydrocarbon whose chemical behavior vividly illustrates many of the principles discussed above. Due to its formal 4n $\pi$-electron configuration ($n = 2$) and enforced rigid planarity, pentalene serves as a prototypical example of antiaromatic instability. It provides a valuable platform not only for the theoretical and spectroscopic exploration of antiaromaticity but also for the design of functionally modified derivatives with tunable electronic properties, pushing the boundaries of what is chemically possible.

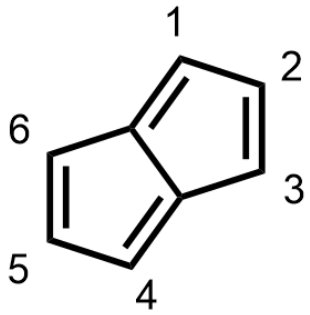


**Figure 1.2**: Structure of pentalene.

Pentalene ($C_8H_6$) consists of two fused five-membered rings, forming an 8 $\pi$-electron system that fulfills all the geometric and electronic conditions for antiaromaticity under Hückel's rule.[36] Its coplanar conformation, often stabilized by a transannular bond that locks its geometry, enables complete $\pi$-delocalization across the entire bicyclic system, which paradoxically contributes directly to its inherent electronic destabilization. The molecule's isolation and direct spectroscopic observation were only accomplished in 1997, when Bally and co-workers successfully generated it by photocleavage of a thermally unstable [2+2] dimer in frozen argon matrices.[37] The resulting infrared spectrum

provided crucial experimental evidence, revealing distinct bond-length alternation —- a key structural marker of antiaromaticity.

Due to its intrinsic antiaromaticity and consequent instability, pentalene, and its derivatives, have long been challenging molecules to study and manipulate, especially in its unsubstituted form. As a result, significant effort —– both experimental and, increasingly, computational —– has been devoted to identifying structural motifs and electronic modifications that can enhance its persistence and suppress its characteristic reactivity.[38],[39],[40],[41],[42],[43] In computational studies, stabilization strategies are often rigorously assessed through analyzing changes in energetic parameters (e.g., heats of formation, dimerization energies), frontier orbital distributions, and aromaticity indices such as NICS[44] and HOMA.[45] A widely employed approach involves steric protection, whereby bulky substituents are strategically introduced near reactive centers of the pentalene core to inhibit intermolecular interactions, particularly dimerization. This strategy has been successfully demonstrated in analogous $\pi$-systems, such as pentacene derivatives, where it can effectively raise the energy barrier to degradation reactions, although steric shielding alone is often insufficient for long-term stabilization.[36],[46] Another highly effective route involves electronic stabilization through annelation with aromatic or extended conjugated units.[47] In pentalene derivatives, fusion with benzene or larger acenes can significantly attenuate antiaromatic destabilization by enabling the delocalization of electron density into the flanking aromatic rings. Such annelated systems —– e.g., dibenzopentalenes —– exhibit improved thermodynamic stability and often display reduced diradical character, findings consistently supported by both spectroscopic data and quantum chemical calculations.[36],[48] A third crucial category of stabilizing strategies includes push—pull substitution, where electron-donating and electron-withdrawing groups (EDG and EWG) are strategically introduced across the $\pi$-system to induce polarization. This deliberate modulation of the electronic landscape can profoundly alter the energy levels of the HOMO and LUMO, influence local and global ring current responses, and strategically affect the aromaticity across the fused rings. Computational evaluations of these subtle yet powerful electronic effects have become critical for identifying promising candidates for synthesis and for accurately predicting their electronic behavior in advanced optoelectronic applications. Together, these computationally accessible modifications offer a rich and versatile platform for exploring how inherently antiaromatic systems like pentalene can be transformed into functional, tunable molecules suitable for integration into cutting-edge materials science and molecular electronics.[49],[50]

## 1.3 Reactivity and dimerization of pentalene

The remarkable reactivity of pentalene arises as a direct consequence of its antiaromatic electronic structure. As a formal 4n $\pi$-electron system with enforced planarity, pentalene intrinsically resides in a high-energy electronic state that strongly favors chemical transformation to relieve the pervasive antiaromatic strain. This inherent reactivity manifests in both profound ground-state instability and a pronounced tendency to undergo facile structural rearrangements or redox-driven changes that effectively stabilize the $\pi$-system by altering its electronic count or disrupting its cyclic conjugation.[36],[51]

In its unsubstituted form, pentalene cannot be isolated under ambient conditions due to its rapid decomposition and immediate dimerization, which occurs even at cryogenic temperatures. The characteristic low HOMO–LUMO gap and strong paratropic ring current, both hallmarks of antiaromatic compounds, collectively contribute to its high sensitivity toward both nucleophilic and electrophilic reagents. While electrophilic substitution reactions are relatively rare due to competing decomposition pathways, pentalene and its derivatives can nonetheless participate in diverse transformations when electronically stabilized or sterically protected.[36] Theoretical studies have also consistently pointed to the crucial involvement of triplet excited states and diradical intermediates in pentalene's reaction mechanisms.[37] This includes its photoinduced reactivity, in which pentalene may exhibit transient aromatic character in the lowest triplet state, a phenomenon consistent with Baird's rule. Although direct photochemical studies on parent pentalene remain scarce due to its extreme instability, computational models robustly suggest that excited-state aromaticity may play a critical role in modulating its reactivity, particularly in $\pi$-stacked or substituted systems. As such, the reactivity of pentalene fundamentally reflects its intrinsic desire to escape antiaromatic destabilization —— either by structural rearrangement, redox-driven $\pi$-electron count adjustment, or direct chemical reaction with external species. Among these various pathways, the most well-known and thermodynamically favorable pathway for this escape is the [2+2] cycloaddition dimerization (Figure 1.3), which thus serves as a primary mechanistic and conceptual entry point for deeper theoretical analysis.

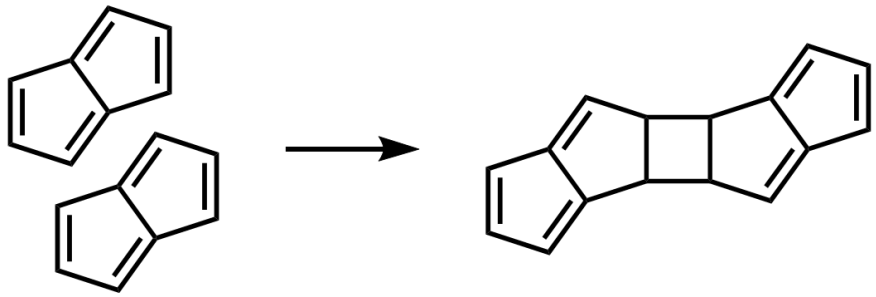

**Figure 1.3**: Dimerization of pentalene.

Among the various chemical transformations available to relieve antiaromatic destabilization, dimerization stands out as the primary and most facile reaction pathway for parent pentalene. At temperatures above –196 °C, unsubstituted pentalene undergoes a rapid and spontaneous [2+2] cycloaddition, forming a non-aromatic dimer with a characteristic pentafulvene-like structure. This remarkable speed and spontaneity underscore the extreme reactivity of the antiaromatic monomer and its strong driving force towards stabilization. This remarkable speed and spontaneity underscore the extreme reactivity of the antiaromatic monomer and its strong driving force towards stabilization. This crucial relationship between the intrinsic thermodynamic stability of reactants and the kinetic barrier to their transformation is elegantly captured by the Bell-Evans-Polanyi (BEP) principle (also known as the Bama–Hapothle relationship).[52] The BEP principle posits that for a family of analogous chemical reactions, there exists a linear correlation between the reaction's activation energy ($\Delta G^{\ddagger}$) and its overall reaction enthalpy (or free energy, $\Delta G$). In essence, the more exergonic (i.e., thermodynamically favorable) a reaction is, the lower its activation energy tends to be, assuming a consistent transition state structure within the series. For pentalene, its profound antiaromatic destabilization results in a significantly elevated ground-state energy. This inherently high energetic starting point means that the dimerization reaction, leading to a much more stable, non-antiaromatic product, exhibits a large and highly favorable $\Delta G$. According to the BEP principle, this substantial thermodynamic driving force directly translates into a remarkably low activation barrier for the [2+2] cycloaddition, explaining its facile and spontaneous nature even at cryogenic temperatures. Consequently, a deep understanding of this thermodynamic-kinetic interplay, guided by the BEP principle, is fundamental for rationalizing pentalene's characteristic reactivity. It also provides a powerful predictive framework for designing derivatives with enhanced kinetic stability: any strategic

modification that mitigates the monomer's antiaromatic character and thus reduces the thermodynamic driving force for dimerization should, by extension, lead to a higher activation barrier, thereby prolonging its lifetime and potentially enabling its isolation under less extreme conditions.

Complementing this energetic perspective, the Hammond–Leffler Postulate (HLP) provides crucial insight into the structural characteristics of the transition state.[53],[54] The HLP states that the transition state of a reaction will structurally resemble the species (either reactant or product) to which it is closer in energy along the reaction coordinate. In practical terms, for a highly exergonic reaction like the dimerization of pentalene, where the transition state is significantly closer in energy to the high-energy antiaromatic monomer than to the more stable dimeric product, the HLP predicts an "early" transition state. This implies that the transition state's geometry, bond lengths, and electronic distribution will closely resemble the reactants. Specifically, the newly forming bonds (e.g., in the [2+2] cycloaddition) are only minimally developed, and the electronic reorganization to alleviate the antiaromatic strain is just beginning. This limited requirement for structural and electronic rearrangement to reach the transition state directly contributes to the exceptionally low activation barrier, making the dimerization of pentalene extraordinarily rapid and spontaneous. Conversely, for endergonic reactions, the transition state would be "late", structurally resembling the products. This powerful postulate, therefore, offers a vivid molecular picture that aligns perfectly with the observed kinetic lability of antiaromatic pentalene, highlighting how its inherent instability drives it through an energetically facile, reactant-like transition state. As expected, the HLP and the MHP are usually related.[55]

Complementing the structural insights provided by the Hammond–Leffler Postulate, the Global Electrophilicity Index (GEI) offers an additional quantitative descriptor to assess the reactivity and electronic predisposition of the pentalene monomer and its derivatives. The GEI is defined as in Eq. 1.2.

$$\omega = \frac{\mu^2}{2\eta} \tag{1.2}$$

Where $\mu$ is the electronic chemical potential and $\eta$ the chemical hardness, provides a measure of a molecule's ability to accept electrons upon interaction with a nucleophilic partner.[56],[57] Higher GEI values indicate a stronger electrophilic character, which in the context of pentalene, directly relates to its tendency to undergo rapid transformations to relieve antiaromatic strain.

In parallel, the Minimum Electrophilicity Principle (MEP) posits that systems naturally evolve toward minimizing their global electrophilicity, thereby achieving greater electronic stability.[58] Applied to the pentalene dimerization process, this principle suggests that the antiaromatic monomer—characterized by a relatively high electrophilicity due to its strained electronic structure—will spontaneously transform into a more electronically stable dimer with lower electrophilicity. This theoretical framework not only supports the observed strong thermodynamic driving force for dimer formation but also complements the GEI analysis, offering a consistent electronic rationale for the exceptionally high reactivity of pentalene and its derivatives. Together, these concepts reinforce the importance of global electronic descriptors in rationalizing and predicting the reactivity patterns of antiaromatic systems.

Interestingly, the very same antiaromatic character that drives pentalene to dimerize can be either exploited or effectively suppressed through clever chemical design. Substituted and annelated pentalene derivatives —- such as dibenzo[a,e]pentalenes -— have been shown to resist dimerization due to a combination of both steric and electronic stabilization.[59] Conversely, polycyclic pentalenes with enhanced antiaromaticity have been strategically synthesized to probe the fundamental limits of this reactivity and to explore their potential as functional materials with narrow band gaps and unique optical responses.[60] Dimerization, therefore, serves not only as a mechanistic outlet for antiaromatic instability, providing a crucial pathway for molecular stabilization, but also as a fundamental benchmark reaction in evaluating how structural modifications effectively modulate the intrinsic reactivity of pentalene-based systems. Its comprehensive study provides essential insights into the intricate interplay between antiaromaticity, excited-state reactivity, and molecular stability, forming a key focus in both experimental and computational investigations of $\pi$-conjugated frameworks.

## 1.4 Research gap and thesis aims

Despite the rich theoretical interest in antiaromatic systems and their unique chemical behavior, the detailed computational investigation of pentalene dimerization remains notably underexplored. While numerous studies have extensively focused on the electronic structure, stability, and aromaticity indices of pentalene and its various derivatives, comparatively few have systematically addressed the specific reaction pathways, the comprehensive energy profiles, or the precise transition-state characteristics governing its [2+2]

cycloaddition. This lack of detailed mechanistic insight is particularly surprising given the central and defining role that dimerization plays in shaping the molecule's chemical fate and limiting its isolation. As such, a focused theoretical analysis of pentalene dimerization offers a valuable and timely opportunity to fill this critical gap in understanding, clarify existing mechanistic ambiguities, and contribute broadly to our fundamental knowledge of antiaromatic reactivity and characteristics in complex polycyclic hydrocarbons.

The primary objective of this thesis is to theoretically investigate the dimerization of pentalene and its derivatives through advanced computational quantum chemical methods, with a particular focus on how thermodynamic stability, kinetic accessibility, and local (anti)aromatic character collectively govern this pivotal transformation. By systematically analyzing a diverse range of substituted pentalenes, this study seeks to elucidate the intricate structure —- reactivity relationships that dictate whether the monomer persists as a stable species or readily undergoes dimerization under given conditions. Special attention is given to the sophisticated interplay between frontier molecular orbital topology, the precise reaction energetics (including both ground states and transition states), and various aromaticity indices, which together fundamentally shape the reaction pathway. The ultimate goal is to identify how specific substituent effects modulate the antiaromaticity of the monomer, influence the stabilization or destabilization of the intervening transition states, and ultimately determine the thermokinetic feasibility of the overall dimerization process. In doing so, this work aims to contribute both novel mechanistic insight and a robust predictive framework for designing antiaromatic systems with finely tunable reactivity profiles, which is essential for unlocking their potential application in emerging fields of materials science and advanced molecular electronics.

# Chapter 2

# Objectives

The overarching aim of this thesis is to perform a computational investigation of the dimerization of pentalene, focusing on how structural substitution with electron-donating (EDG) and electron-withdrawing groups (EWG) affects this reaction. Through systematic modification of the pentalene framework, this work seeks to understand how substituents influence the thermodynamic and kinetic aspects of the dimerization process, as well as the underlying electronic and aromatic character of both monomeric and dimeric species.

To achieve this, the study evaluates how various substituents introduced at key positions on the pentalene scaffold impact the activation barriers, reaction Gibbs energies, and frontier molecular orbital distributions. In parallel, the (anti)aromatic character of these systems is quantified using established computational descriptors. The ultimate objective is to uncover structure–property–reactivity relationships that explain how substitution modulates the balance between antiaromatic strain and dimerization propensity, and to contribute generalizable insights into the behavior of antiaromatic $\pi$-systems under electronic perturbation.

# Chapter 3

# Methodology

## 3.1 Computational details

All quantum chemical calculations presented in this thesis were performed using the Gaussian 16 software package.[61] The molecular geometries of all studied pentalene monomers, substituted pentalene derivatives, their corresponding dimeric products, and the relevant transition states (TSs) were fully optimized without imposing any symmetry constraints.

The chosen level of theory for all optimizations and subsequent analyses was Density Functional Theory (DFT), utilizing the B3LYP hybrid functional.[62],[63],[64],[65] B3LYP is a widely employed functional in computational organic chemistry, known for its good balance between computational cost and accuracy for predicting molecular structures, reaction energies, and vibrational frequencies in organic systems. To account for dispersion interactions, which are crucial for accurately describing non-covalent interactions such as $\pi$-stacking in the pentalene dimers, Grimme's third-generation empirical dispersion correction with Becke-Johnson damping (D3BJ) was included.[66]

For the atomic orbital basis set, the 6-311++G** basis set was employed. This triple-zeta basis set includes diffuse functions ('++') on all atoms (heavy and hydrogen atoms), which are essential for accurately describing anionic species, lone pairs, and, importantly, long-range electron distribution effects crucial for weak intermolecular interactions and extended $\pi$-systems. Additionally, it incorporates polarization functions ('**') on all atoms (heavy atoms and hydrogen atoms), allowing for a more flexible description of electron density in chemical bonds and improving the accuracy of geometry optimiza-

tions and energy calculations.

Following geometry optimizations, vibrational frequency calculations were performed at the same level of theory (B3LYP/6-311++G** with GD3BJ dispersion) for all optimized structures. These calculations served two primary purposes: first, to confirm the nature of each stationary point on the potential energy surface, whereby minima were characterized by the absence of imaginary frequencies and transition states were identified by the presence of exactly one imaginary frequency; and second, to obtain zero-point vibrational energies (ZPVEs) and thermal corrections to energy, enthalpy, and Gibbs energy at 298.15 K and 1 atm, which were subsequently used to report thermochemical data.

The connectivity of each identified transition state to its corresponding reactant and product was rigorously verified by performing Intrinsic Reaction Coordinate (IRC) calculations.[67] These calculations trace the minimum energy pathway downhill from the transition state in both forward and reverse directions, providing clear evidence that the optimized transition state indeed connects the desired reactant and product species on the potential energy surface.

## 3.2 Aromaticity indicators

To quantitatively assess the aromatic or antiaromatic character of the studied pentalene systems, two complementary electron delocalization-based indices were employed: the Multicenter Index (MCI) and the $I_{ring}$ index.

The Multicenter Index (MCI) is a robust aromaticity descriptor derived from multicenter electron sharing, which provides a direct measure of the degree of $\pi$-electron delocalization within a cyclic framework.[68] Higher MCI values generally indicate enhanced aromaticity (or stronger cyclic delocalization), while low or negative values are characteristic of antiaromatic or localized structures. The Iring index, on the other hand, is closely related to the MCI and is specifically designed to quantify the cyclic delocalization of electrons within a defined ring or set of atoms.[69] This index further refines the assessment of local aromaticity contributions and is particularly informative when evaluating fused or polycyclic systems like pentalene derivatives.

All MCI and Iring calculations were performed using the ESI-3D method as implemented in the open-source Python package ESIpy.[70] This program allows for the efficient computation of multicenter electron sharing indices.

These electron delocalization-based aromaticity indices provide a deeper understanding of the electronic reorganization accompanying pentalene dimerization and the influence of substituents on local and global (anti)aromatic character. Together with magnetic and structural criteria, MCI and $I_{ring}$ form a comprehensive set of tools to characterize aromaticity trends throughout this study.

# Chapter 4

# Theoretical study and characterization of pentalene dimerization

To initiate this study, it is essential to first analyze the structure of pentalene itself. As discussed in previous sections, pentalene is composed exclusively of carbon and hydrogen atoms, arranged in two fused five-membered rings. Although pentalene serves as the main subject of this work, it is insightful to begin by considering the simpler reference system of cyclobutadiene.

The dimerization of cyclobutadiene and pentalene proceeds through a [2+2] cycloaddition mechanism, in which two $\pi$-electrons from each monomer are used to form new $\sigma$-bonds, creating a four-membered ring between them.[71] Although it is formally forbidden by the Woodward-Hoffmann rules,[72] this [2+2] reaction is characteristic of antiaromatic systems that seek to relieve their destabilizing electron delocalization by forming $\sigma$-bonds at reactive $\pi$-sites. In the case of pentalene, the reaction typically occurs at the most electron-rich double bonds, usually across the central 1,3-positions (see Figure 1.2) of each five-membered ring. The resulting product is a non-aromatic or weakly conjugated dimer with a pentafulvene-type topology, significantly reducing its antiaromatic character compared to the monomer. This [2+2] cycloaddition is thermodynamically favored due to the release of antiaromatic strain.

Using the computational methodology described in the previous section, an initial attempt was made to study cyclobutadiene. However, due to its extreme instability, cy-

clobutadiene readily dimerizes and could not be reliably optimized, as the monomeric species and transition state calculations failed to converge. This observation is consistent with the study carried out by Mesías Orozco-Ic and Dage Sundholm in 2023, which investigated the dimerization of cyclobutadiene.[73] Their work concluded that the face-to-face stacked dimer of cyclobutadiene is not a true minimum but rather a transition state characterized by imaginary vibrational frequencies. The tendency of these dimers is to rearrange and form a cubane-type structure, which represents the global energy minimum.

In contrast, the present work focuses on the dimerization of pentalene. Similar to cyclobutadiene, pentalene exhibits intrinsic instability that makes it highly susceptible to dimerization reactions. This section aims to analyze the possible dimerization pathways of pentalene and to characterize the resulting dimeric structures, with the goal of understanding how antiaromaticity influences these processes.

Before discussing the specific reactant geometries and product structures, it is important to outline the general mechanism governing pentalene dimerization (Figure 4.1). In line with its strong antiaromatic character and high reactivity, pentalene undergoes dimerization via a [2+2] cycloaddition mechanism, a well-established pathway for $\pi$-conjugated systems seeking to relieve electronic strain. This reaction involves the direct overlap of two $\pi$-systems, resulting in the formation of two new $\sigma$-bonds and a four-membered ring, effectively converting $\pi$-electron density into more stable covalent bonding. The process is typically concerted but can proceed asynchronously, reflecting differences in bond formation rates along the reaction coordinate. For antiaromatic systems like pentalene, this transformation leads to a significant reduction in overall electronic energy. As such, dimerization serves as a highly favored escape route from antiaromatic instability and represents a critical mechanistic entry point for understanding and rationalizing the reactivity patterns of pentalene and its derivatives.

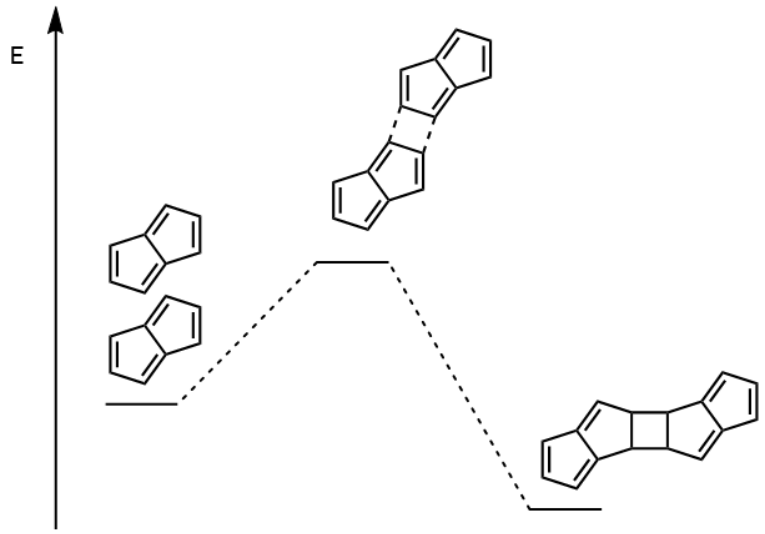


**Figure 4.1**: Proposed general mechanism for pentalene dimerization via [2+2] cycloaddition pathway.

Preliminary calculations involving two approaching pentalene monomers yielded two distinct results. The first result corresponds to a structure in which the two pentalene subunits are stacked on top of each other, maximizing $\pi$–$\pi$ stacking interactions, as illustrated in Figure 4.2. In this configuration, the subunits maintain an almost parallel orientation with a characteristic intermolecular distance, stabilized by non-covalent $\pi$–$\pi$ interactions. Although these interactions are much weaker than covalent bonds, they are fundamental in many chemical and biological contexts and provide some degree of stability to the stacked dimer.The stabilization energy of this complex was calculated as $E(dimer) - 2 \cdot E(monomer)$, representing the energy difference between the dimer and two isolated monomers.

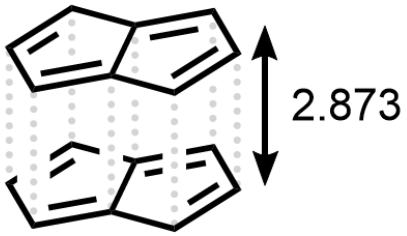


**Figure 4.2**: Pentalene structure in $\pi$-$\pi$ stacking position. (distance in Å)

The second result corresponding to an [8+8] forbidden cycloaddition revealed a markedly different structure, which can be compared to that of cubane. As shown clearly in Figure 4.3, in this configuration all carbon atoms from both pentalene subunits are connected via covalent bonds, forming a dense and closed three-dimensional network. This extended connectivity leads to a molecular topology reminiscent of the symmetry and angular strain found in cubane, with significant implications for its stability.

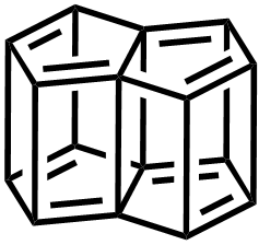

**Figure 4.3**: Pentalene structure in cubane-like position.

A comparison of the relative energies of these two dimeric structures reveals a substantial difference. The cubane-like structure is dramatically less stable than the stacked configuration, with an energy difference of 126.23 kcal/mol. This large energetic disparity suggests that the formation of multiple direct covalent bonds between pentalene subunits imposes considerable strain and results in a highly unfavorable configuration, making it extremely difficult to form or maintain under normal conditions.

For the continuation of this study, only the first structure will be considered, given its significantly higher relative stability.

In the transition state structure, one observes a characteristic feature common to [2+2] cycloaddition reactions. It is important to highlight that this specific reaction proceeds through an asynchronous concerted [2+2] cycloaddition mechanism. This means that although the formation of the two new covalent bonds occurs within a single mechanistic step, the process is neither perfectly simultaneous nor fully symmetric (Figure 4.4). In fact, at the point of highest energy corresponding to the transition state, one bond is more developed than the other. This asynchronous nature has been meticulously confirmed through the calculation of the intrinsic reaction coordinate (IRC), which allows the most energetically favorable path from the transition state toward both reactants and products to be traced.

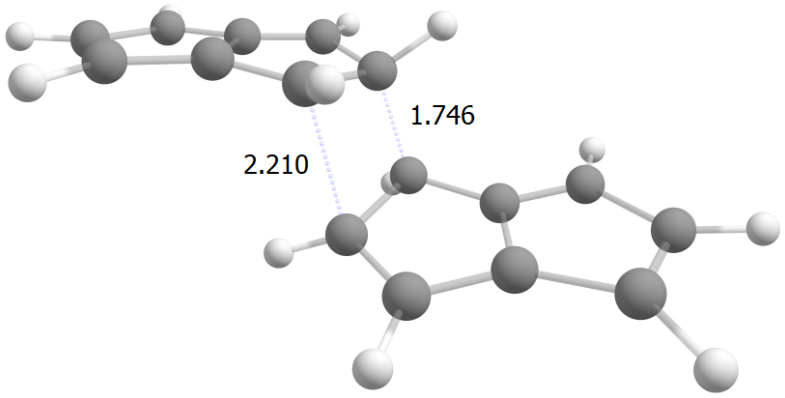


**Figure 4.4**: Transition state structure of pentalene dimerization showing unequal formation of the two new $\sigma$-bonds, consistent with an asynchronous concerted mechanism. (bond distance in Å)

Once the possible structures of the reactants and the transition state have been analyzed, the structure of the product can be explored.

With the context established on the instability and dimerization behavior of cyclobutadiene, the study conducted by Houk and Li in 1996 on its dimerization provides a crucial analogy for predicting the stable product form of pentalene dimerization.[71] Their study demonstrated that cyclobutadiene dimerizes without a significant potential energy barrier. The *-syn* dimerization, in particular, is strongly favored and was predicted to have a "negative activation energy", indicating a highly rapid reaction. More importantly, the dimerization pathways of cyclobutadiene lead directly to products where the two subunits are covalently connected, transforming into a strained polycyclic structure. In no case is the final stable product merely a non-covalently $\pi$-stacked dimer.

This observation is highly relevant to the case of pentalene dimerization. Given that both cyclobutadiene and pentalene possess pronounced antiaromatic character, it is reasonable to expect that their intrinsic instability would drive them to react by forming new covalent bonds to relieve this strain. Therefore, if cyclobutadiene readily forms covalently bonded products and does not stabilize as a simple $\pi$–$\pi$ stacked dimer, it can be inferred that the stable product of pentalene dimerization is also unlikely to be a simple non-covalent $\pi$-stacked dimer. Instead, pentalene is expected to favor the formation of a more complex structure in which the two subunits are covalently connected, resulting in a final product with a molecular topology significantly different from mere stacking.

As shown in Figure 4.5, the study on cyclobutadiene dimerization by Houk and Li illustrates the relative energies and geometries associated with the various structures

formed during the process. This representation provides a valuable analogy for anticipating the stability of the pentalene dimer. Given the similarities in reactivity and antiaromatic character of both molecules, understanding the energetic pathways of cyclobutadiene is key to guiding our analysis of pentalene dimerization.

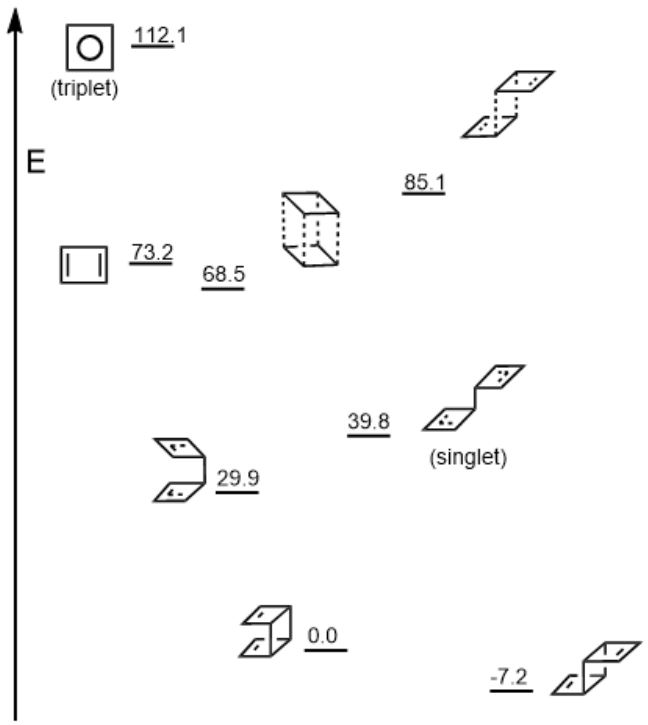


**Figure 4.5**: Scheme (adapted) of relative energies (in kcal/mol) and associated geometries during cyclobutadiene dimerization (Houk and Li, 1996).

Following this, I proceed to study in detail the different forms and stabilities of the pentalene dimer, applying insights gained from the analogy with cyclobutadiene.

Detailed calculations were performed for the lowest-energy structures of the pentalene dimer, using knowledge derived from analogous studies as a reference. The results reveal the existence of two main arrangements: the conformation in which the two pentalene units are oriented in opposite directions, referred to hereafter as the *trans* conformer (as shown in Figure 4.6), and the conformation where the pentalene units are aligned in the same direction, referred to hereafter as the *cis* conformer (depicted in Figure 4.7).

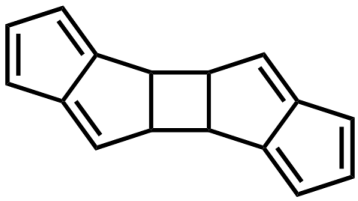

**Figure 4.6**: Schematic representation of the *trans* conformer of the pentalene dimer, illustrating the two pentalene units oriented in opposite directions.

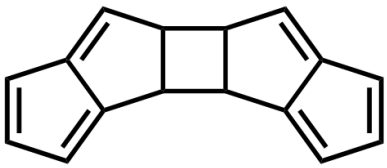

**Figure 4.7**: Schematic representation of the *cis* conformer of the pentalene dimer, depicting the two pentalene units aligned in the same direction.

In comparing their relative stabilities, it has been determined that the *trans* configuration is slightly more stable than the *cis* arrangement, with an energy difference of only 0.22 kcal/mol. This small difference suggests that both conformations could potentially coexist or be accessible under similar conditions. However, when analyzing the energetic barriers for interconversion or formation, it was observed that the energetic barriers that lead to the formation of the *cis* and *trans* isomers exhibits a barrier that is 1.75 kcal/mol higher, indicating that formation or transition through the *cis* conformer may be slightly less kinetically favored.

# Chapter 5

# Functional group effects on pentalene dimerization

After having thoroughly analyzed the dimerization of unsubstituted pentalene and established analogies with cyclobutadiene, the next step in this study is to investigate how the introduction of functional groups can modulate this process. Functionalization of antiaromatic molecules, such as pentalene, is a widely used strategy to modify their stability, electronic properties, and consequently, their intrinsic reactivity. In this section, we explore the impact of various electronic and steric substituents on the tendency of pentalene to dimerize, focusing on the geometries and stabilities of the resulting dimeric products. Our aim is to search for substituents that avoid dimerization, and consequently, the optoelectrical properties due to antiaromaticity of these substituted pentalenes are mostly preserved, so they can be used in optoelectronic devices.

For this purpose, the recent study by Sanderson et al.[36] on the reversible formation of tetraphenylpentalene has been taken into account as a reference point. In the present work, the investigation focuses on pentalene structures functionalized with specific groups that allow both electronic (donor/acceptor) and steric effects to be analyzed. In particular, the selected functional groups include hydroxyl (–OH), cyano (-CN), methoxycarbonyl (-COOMe), formyl (–CHO), and tert-butyl (-t-Bu), whose structures are shown in Figure 5.1, to evaluate their influence on the dimerization of pentalene.

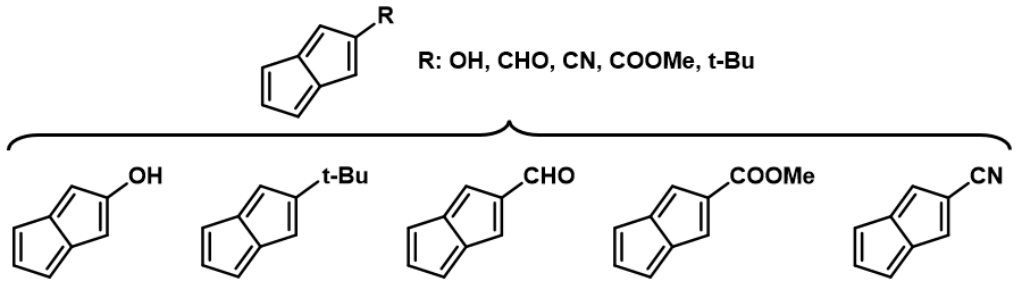


**Figure 5.1**: Structures of pentalene substituted with hydroxyl (–OH), cyano (-CN), methoxycarbonyl (-COOMe), formyl (–CHO), and tert-butyl (-t-Bu) groups used in this study.

To address the study of pentalene dimerization with functional groups, two distinct reaction pathways have been considered, leading to dimeric products with different stereochemical orientations. These pathways are directly influenced by the position of the substituents on the monomeric pentalene structure and their interactions during dimer formation.

The first pathway leads to a product in which the substituents point outward from the dimer. This configuration minimizes steric interactions between the functional groups of the two subunits, potentially facilitating the approach and formation of the new bonds. In contrast, the second dimerization pathway results in a disposition in which the functional groups are directed toward the interior cavity of the dimer. This internal orientation introduces significant steric hindrance, as the substituents may collide or come too close to each other, affecting both the activation barrier and the final stability of the product. Both pathways are crucial for understanding the influence of steric effects on dimerization reactivity, as clearly illustrated schematically in Figure 5.2.

In addition to these two main orientations, there are two further theoretical possibilities: one where both substituents are oriented inward but point in the same direction, and another mixed configuration where one substituent points inward and the other outward. While these additional arrangements could potentially offer further insight into the steric and electronic interplay during dimerization, they have not been explored in the present study due to time constraints. Moreover, the discussion of the alternative cis dimerization conformations is addressed in detail in a subsequent section.

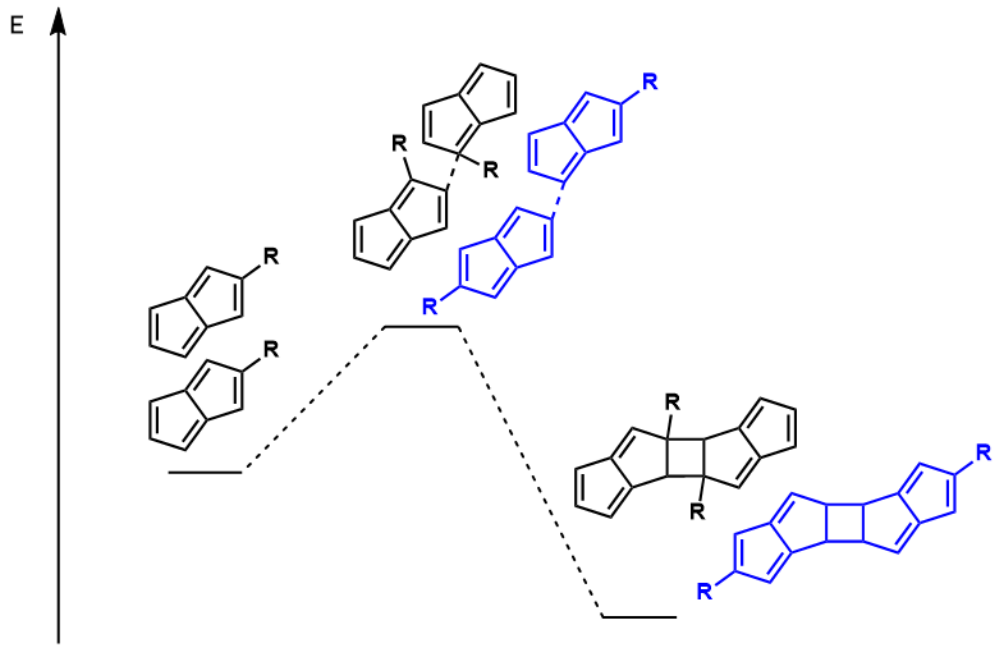


**Figure 5.2**: Schematic representation of the two dimerization pathways of substituted pentalene, showing the orientation of functional groups toward the exterior (blue) and toward the interior (black) of the dimer.

Once these two stereospecific pathways for substituted pentalene dimerization were defined, computational calculations were carried out to determine the relative energies of the resulting products and the corresponding activation barriers for each selected functional group. The results obtained for each substituent, for both the pathway with substituents pointing outward and the one with substituents oriented inward, are summarized in Table 5.1. It is important to note that all energies presented in this table are relative to the separated substituted pentalene monomers. These energetic values allow for direct evaluation of the influence of electronic effects (such as donor or acceptor character) and steric effects (derived from the bulkiness of the substituent) on the preference for each dimerization pathway and on the final stability of the dimeric product.

**Table 5.1**: Relative Gibbs energies (kcal/mol) of substituted pentalene dimers for the "exterior" (ext) and "interior" (int) pathways, and corresponding transition state (TS) energies.

| Substituent | $\Delta G_{dim,ext}$ | $\Delta G_{dim,int}$ | $\Delta G_{TS,ext}$ | $\Delta G_{TS,int}$ |
|---|---|---|---|---|
| –H (pentalene) | –18.04 | — | 21.88 | — |
| –OH | –19.26 | –12.42 | 22.28 | 19.95 |
| –CN | –14.81 | –6.35 | 23.30 | 20.86 |
| –COOMe | –12.62 | –8.93 | 24.18 | 25.87 |
| –CHO | –13.63 | –5.47 | 21.69 | 19.08 |
| –t-Bu | –20.69 | –11.50 | 20.75 | 31.80 |

A key observation from these results is that the formation of substituted pentalene dimers is generally a thermodynamically favorable (exothermic) process. This is reflected in the negative Gibbs free energies of most dimer products relative to the separated monomers, confirming that dimerization acts as a driving force to relieve the antiaromatic character of pentalene monomers through the formation of more stable $\sigma$-bonds, as previously discussed.

When comparing the unsubstituted pentalene with its functionalized derivatives, important differences emerge that highlight the influence of electronic and steric effects on dimerization. The unsubstituted pentalene exhibits a strongly exergonic dimerization ($\Delta G_{dim}$ = –18.04 kcal/mol) and a relatively moderate transition state barrier ($\Delta G_{TS}$ = 21.88 kcal/mol), reflecting its strong intrinsic tendency to alleviate antiaromatic destabilization via rapid dimerization.

Among the substituted systems, the tert-butyl (–t-Bu) group displays the most negative dimerization energy for the exterior pathway ($\Delta G_{dim,ext}$ = –20.69 kcal/mol), suggesting a highly thermodynamically favored product. However, the corresponding barrier for the interior pathway is the highest observed ($\Delta G_{TS,int}$ = 31.80 kcal/mol), clearly demonstrating that the large steric hindrance of –t-Bu significantly impedes the approach of monomers in confined geometries. This indicates that while the final dimer is strongly stabilized, the reaction pathway is kinetically hindered for inward configurations.

In contrast, electron-withdrawing substituents like cyano (–CN) and ester (–COOMe) groups exhibit less negative dimerization energies (e.g., $\Delta G_{dim,ext}$ = –14.81 and –12.62 kcal/mol, respectively) and higher transition state barriers for exterior pathways ($\Delta G_{TS,ext}$ = 23.30 and 24.18 kcal/mol). These findings suggest that strong electron-withdrawing groups tend to decrease the thermodynamic driving force for dimerization

and increase kinetic barriers, effectively reducing the overall reactivity.

For the formyl (–CHO) and hydroxyl (–OH) substituents, the dimerization remains favorable ($\Delta G_{dim,ext}$ = –13.63 and –19.26 kcal/mol), with moderate barriers ($\Delta G_{TS,ext}$ = 21.69 and 22.28 kcal/mol). This indicates that these groups, while still stabilizing the product relative to monomers, impose moderate kinetic hindrance. Notably, the hydroxyl derivative shows one of the most balanced profiles, combining favorable thermodynamics with manageable kinetic access, consistent with its smaller size and ability to engage in possible weak polar interactions.

Overall, these trends reveal that substituents can either hinder or facilitate dimerization depending on their electronic and steric nature. Large, bulky groups such as –t-Bu primarily hinder the reaction kinetically through severe steric repulsion in the transition state, particularly in interior approaches. Electron-withdrawing substituents reduce both the thermodynamic favorability and kinetic accessibility by stabilizing the monomeric antiaromatic form, thus reducing the driving force for $\sigma$-bond formation.

In conclusion, while the overall tendency to relieve antiaromaticity via dimerization is conserved across all systems, the extent to which substituents modulate this process is significant. Bulky or strongly electron-withdrawing substituents clearly emerge as the primary factors impeding dimerization, either by raising activation barriers, reducing exergonicity, or both. This detailed analysis provides a powerful framework for designing pentalene derivatives with controlled reactivity, either to stabilize the monomeric antiaromatic form or to promote dimer formation selectively.

Analyzing the thermodynamic stability of the dimers ($\Delta G_{\mathrm{dim,ext}}$ vs. $\Delta G_{\mathrm{dim,int}}$), one can observe that in almost all cases, the "exterior" pathway is thermodynamically more favorable, indicating that arranging the substituents away from the dimer cavity reduces steric strain and favors the final product's stability. This trend is particularly pronounced for the tert-butyl group (-t-Bu), a well-known electron-donating group (EDG) with high steric bulk. The "exterior" dimer is significantly more stable (–20.69 kcal/mol), while the "interior" form is less stabilized (–11.50 kcal/mol relative to monomers), with a difference of nearly 10 kcal/mol favoring the exterior configuration. This highlights the severe internal steric repulsion encountered in the "interior" conformation. The hydroxyl group (–OH), another EDG though considerably smaller than -t-Bu, also shows a clear preference for the "exterior" pathway (–22.87 kcal/mol), being 9.95 kcal/mol more stable than the "interior" form (–15.92 kcal/mol). This may suggest, in addition to steric hindrance, the presence of unfavorable electronic or intramolecular hydrogen bonding interactions in the interior configuration.

Interestingly, when analyzing the kinetic behavior (transition state barriers) in parallel, some substituents show lower activation barriers in the "interior" pathway despite its thermodynamic disadvantage. This observation can be rationalized by examining the frontier molecular orbitals in the transition state structures. For example, in the case of the cyano group (–CN), detailed orbital visualizations reveal that the nitrogen lone pair and the $\pi$ system of the cyano substituent engage in significant orbital overlap with the approaching pentalene fragment when oriented inward. As illustrated in Figure 5.3, this mixing leads to partial delocalization and stabilizes the developing transition state, effectively lowering the kinetic barrier for the interior arrangement. Such an electronic interaction is largely absent when the substituent is directed outward, where it remains electronically isolated from the reactive core. This result highlights how local electronic effects and substituent position can modulate the balance between thermodynamic and kinetic control, ultimately influencing the preferred dimerization pathway of substituted pentalene systems.

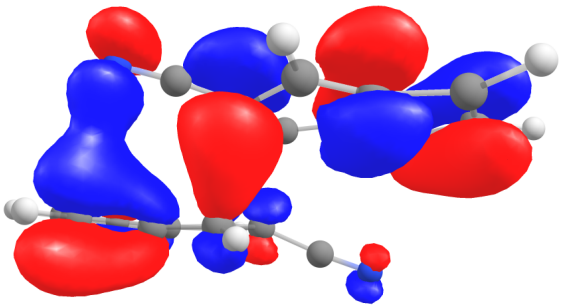

**Figure 5.3**: Visualization of the HOMO in the transition state structure of the cyano-substituted pentalene dimer (interior configuration).

In summary, these results demonstrate that substituted pentalene dimerization is governed by a delicate balance between steric effects and transition state factors, and that the electronic nature of the substituent can modulate this balance. While thermodynamics generally favors the "exterior" conformation to minimize steric hindrance, the kinetics of the reaction may lead to a preference for the "interior" pathway for less bulky substituents. This competition between thermodynamic and kinetic control is fundamental to understanding the selectivity of these reactions and opens avenues for further studies on electronic factors stabilizing interior transition states. The generally exothermic nature of these dimerizations underscores the high reactivity of pentalene as an antiaromatic molecule seeking stabilization through dimer formation.

After exploring in detail the influence of functional groups on the "exterior" and "interior" dimerization pathways, this study broadens its scope to consider other possible geometric configurations that pentalene molecules may adopt during the dimerization process. The complexity of cycloaddition reactions often lies in the multiplicity of possible monomer approaches, leading to products with diverse topologies and stabilities.

Now, I will focus on the analysis of the two alternative dimerization arrangements that go beyond the simple orientation of substituents in the final dimer, as I commented in previous sections. These new reaction pathways, involving different intermolecular alignments of the two pentalene monomers, have been investigated to determine their energetic viability and the nature of the resulting products, the already studied conformation will be called the *trans* product and the following one will be called the *cis* product. The two arrangements considered are illustrated in Figure 5.4, showing the approach geometries of the monomers and potential bond formations. The goal is to determine whether these alternative pathways can compete with those previously studied and how the inherent antiaromaticity of pentalene drives the formation of dimeric structures with specific features.

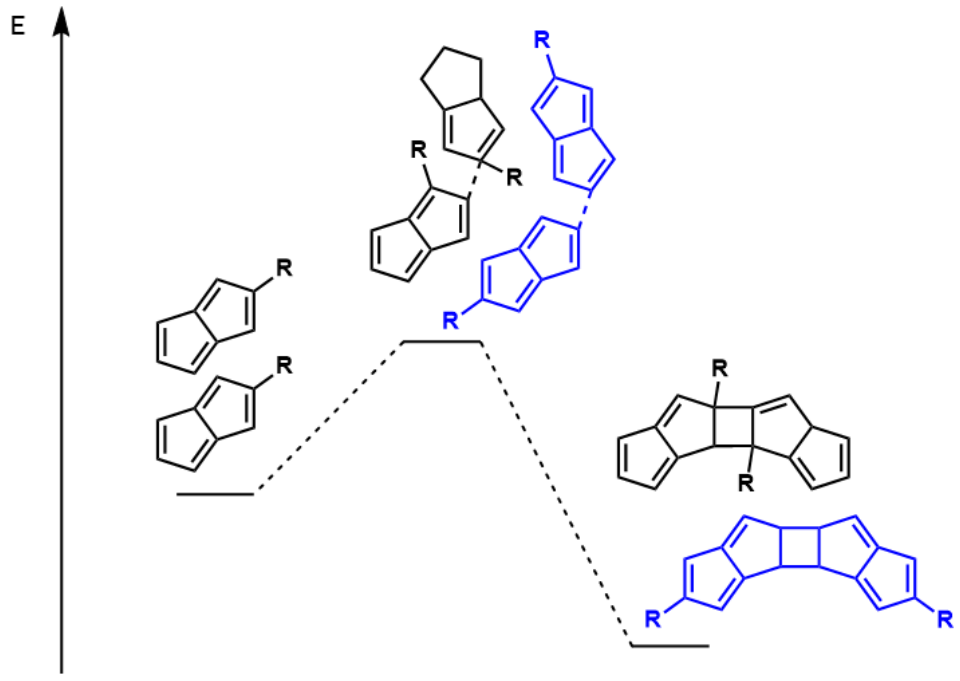


**Figure 5.4**: Schematic representation of two alternative approaches for pentalene dimerization, showing different monomer alignments and potential formation of products with varied topologies.

Now, considering these two conformational frameworks — the previously studied *trans* arrangement and the *cis* arrangement examined here — the analysis of functional substituents has been repeated for both the "interior" and "exterior" orientations within each framework. The resulting data are summarized in Table 5.2.

**Table 5.2**: Relative Gibbs energies (in kcal/mol) of substituted pentalene dimers for the "exterior" (ext) and "interior" (int) pathways, and corresponding transition state (TS) energies for the *cis* conformation.

| **Substituent** | $\mathbf{\Delta G_{dim,ext}}$ | $\mathbf{\Delta G_{dim,int}}$ | $\mathbf{\Delta G_{TS,ext}}$ | $\mathbf{\Delta G_{TS,int}}$ |
|---|---|---|---|---|
| –OH | –20.11 | –12.20 | 22.24 | 19.72 |
| –CN | –14.49 | –5.74 | 25.03 | 24.02 |
| –COOMe | –12.06 | –6.83 | 27.04 | 23.03 |
| –CHO | –14.95 | –3.64 | 24.60 | 23.89 |
| –t-Bu | –18.54 | –6.70 | 21.06 | 29.64* |

From the data collected in Table 5.2, several important conclusions can be drawn regarding the influence of functional substituents on the alternative dimerization arrangements of pentalene.

In general, the *cis* dimerization remains a thermodynamically favorable (exergonic) process for all substituents, as indicated by the negative relative Gibbs free energies ($\Delta G_{dim}$) for both the "exterior" and "interior" pathways. Consistently with the results from the initial conformational study, the "exterior" pathway is more thermodynamically favorable for all substituents considered. This is especially pronounced for the tert-butyl (–t-Bu) and hydroxyl (–OH) substituents, with $\Delta G_{dim,ext}$ values of –18.54 kcal/mol and –20.11 kcal/mol, respectively, compared to –6.70 kcal/mol and –12.20 kcal/mol for the "interior" pathways. This difference underscores the strong steric repulsion and possible unfavorable interactions that arise when bulky or polar substituents are oriented toward the interior cavity of the dimer.

For electron-withdrawing groups such as cyano (–CN), methoxycarbonyl (–COOMe), and formyl (–CHO), the same trend persists, although the differences in stability between the two pathways are somewhat smaller. This suggests that while steric effects remain important, electronic contributions also play a significant role in modulating the relative stabilities of these dimers.

When examining the kinetic aspects, the transition state energies ($\Delta G_{TS}$) reveal a more nuanced picture. For the hydroxyl substituent (–OH), the "interior" transition state

barrier (19.72 kcal/mol) is lower than that for the "exterior" pathway (22.24 kcal/mol), indicating a potential kinetic preference for the interior pathway despite its lower thermodynamic stability. This same tendency is observed for cyano (–CN), methoxycarbonyl (–COOMe), and formyl (–CHO), with slightly lower or comparable barriers for the "interior" configurations. These results suggest that for these less bulky substituents, the reaction may proceed under kinetic control, favoring the formation of "interior" dimers even though the "exterior" products are thermodynamically more stable.

Notably, for the tert-butyl substituent (–t-Bu), the data show a strong preference for the exterior" pathway, not only thermodynamically but also kinetically, as reflected by the lower transition state barrier (21.06 kcal/mol). In the case of the interior" pathway for the *cis* configuration, a fully optimized transition state could not be located, likely due to the severe steric bulk of the tert-butyl group, which significantly hinders the approach of the two monomers in this orientation. Nevertheless, to gain insight into the energy profile, a linear transit scan was performed, revealing an estimated barrier of 29.64 kcal/mol. This markedly higher barrier further confirms that the "interior" pathway is strongly disfavored for –t-Bu, reinforcing the conclusion that steric effects dominate in dictating both the thermodynamic and kinetic preferences for this substituent.

Overall, these findings reinforce the notion that the dimerization of substituted pentalenes is governed by a delicate interplay between steric and electronic effects. The results highlight that while thermodynamics generally drives the system toward "exterior" dimer formation to minimize steric strain, kinetic factors can lead to competing preferences, particularly for smaller or electronically stabilizing substituents. This competition between kinetic and thermodynamic control provides valuable insight into the reactivity landscape of antiaromatic pentalene derivatives and offers a framework for designing substituents to modulate dimerization selectivity and reactivity profiles.

# Chapter 6

# Discussion of electronic and structural factors

After the detailed analysis of the relative stabilities and activation barriers associated with pentalene dimerization in both unsubstituted and substituted systems, it is crucial to extend the discussion to the underlying electronic and geometric factors that govern these observations. In this chapter, I will examine in detail the optimized geometries of the monomers and dimers to understand how structural deformation facilitates or hinders dimerization.

Additionally, I will analyze the evolution of the HOMO–LUMO gap across the different systems and discuss its correlation with chemical reactivity and stability. This analysis will be complemented by evaluating the Maximum Hardness Principle and the Minimum Electrophilicity Principle, providing insights into the global electronic stability trends of each species.

Furthermore, I will explore the relevance of the Bell–Evans–Polanyi relationship (also known as the Bema–Hapothle correlation) and the Hammond–Leffler postulate to rationalize the observed transition state energetics and reaction profiles. Lastly, aromaticity indices, such as MCI and $I_{ring}$, will be computed and discussed to quantify the (anti)aromatic character of the monomeric and dimeric systems, shedding light on how aromaticity influences the overall thermokinetics of the dimerization process.

By integrating geometric, electronic, and aromaticity analyses, this chapter aims to provide a comprehensive mechanistic understanding of the factors modulating pentalene reactivity and to offer a predictive framework for designing future derivatives with

tailored properties.

It is important to emphasize that all these analyses and descriptors have been specifically applied to the *trans* dimer configuration, as it was found to be more stable than the *cis* arrangement. This choice ensures that the derived mechanistic conclusions are based on the most energetically favorable pathway, thereby providing the most relevant insights into the pentalene dimerization process.

## 6.1 HOMO–LUMO gaps and Maxim Hardness Principle

The reactivity of pentalene derivatives is strongly linked to their frontier orbital energies. Here, I will discuss the HOMO–LUMO gap evolution upon dimerization and substitution, which provides a quantitative measure of electronic stabilization and kinetic accessibility. Smaller gaps are typically associated with higher chemical reactivity, and their modulation by substituents offers valuable insight into electronic effects governing dimerization propensity.

The evolution of HOMO–LUMO gaps along the dimerization pathway offers important insights into the electronic reactivity and stabilization of pentalene derivatives. As shown in Table 6.1, all systems exhibit a significant narrowing of the gap when progressing from the monomeric reactant to the transition state, followed by a pronounced widening upon dimer formation.

**Table 6.1**: Calculated HOMO-LUMO energy gaps (in eV) for unsubstituted and substituted pentalene systems.

| **Substituent** | Reactants | | TS | | Dimer | |
|---|---|---|---|---|---|---|
| | int | ext | int | ext | int | ext |
| –H (pentalene) | 2.58 | — | 1.23 | — | 3.75 | — |
| –OH | 2.35 | 2.35 | 1.55 | 1.55 | 3.34 | 3.46 |
| –CN | 2.41 | 2.41 | 2.74 | 1.51 | 3.71 | 3.66 |
| –COOMe | 2.40 | 2.40 | 1.89 | 1.62 | 3.72 | 3.76 |
| –CHO | 2.25 | 2.25 | 1.70 | 1.25 | 3.61 | 3.71 |
| –t-Bu | 2.82 | 2.82 | 1.77 | 1.88 | 3.72 | 3.80 |

For the unsubstituted pentalene, the HOMO–LUMO gap decreases from 2.58 eV in the monomer to 1.23 eV at the transition state, and then expands dramatically to 3.75 eV in the final dimer. This behavior highlights the highly reactive, electronically soft nature of the transition state and the electronic stabilization achieved in the final product.

A similar pattern is observed across substituted systems. For example, the hydroxyl-substituted pentalene (–OH) shows a gap reduction from 2.35 eV in the reactant to 1.55 eV in the transition state (both interior and exterior arrangements), then broadens to 3.34 eV and 3.46 eV in the dimers, respectively. The tert-butyl derivative (–t-Bu) starts with the largest monomeric gap (2.82 eV), yet still exhibits significant narrowing to 1.77 eV (interior) and 1.88 eV (exterior) at the transition state, followed by expansion to 3.72 eV and 3.80 eV upon dimerization.

Interestingly, the cyano-substituted system (–CN) shows an exceptionally large gap in the interior transition state (2.74 eV), suggesting a relatively more stabilized or less reactive transition structure in this particular configuration, likely due to strong electron-withdrawing effects.

Overall, the narrowing of the HOMO–LUMO gap at the transition state consistently indicates a higher electronic reactivity and increased softness, which facilitates the [2+2] cycloaddition. The subsequent widening of the gap in the final dimeric products reflects a transition toward a more electronically stable, less reactive structure, in line with the Maximum Hardness Principle. These trends confirm that both electronic and steric effects introduced by substituents modulate the reactivity pathway and the electronic character of pentalene derivatives during dimerization.

This analysis aligns closely with the Maximum Hardness Principle (MHP), which states that systems tend to evolve toward states of maximum electronic hardness to minimize reactivity and achieve stability. In this context, the increase in hardness from the transition state to the dimer confirms that the pentalene system reorganizes electronically to reduce softness, becoming more rigid and less susceptible to further reactions. This convergence toward higher hardness values underscores why dimerization is strongly favored from an electronic perspective and highlights how substituents can modulate this trend, providing useful design principles for future derivatives.

## 6.2 Global Electrophilicity Index and Minimum Electrophilicity Principle

We evaluate the Global Electrophilicity Index (GEI) as a complementary descriptor to rationalize the reactivity trends of pentalene systems. The principle of minimum electrophilicity further supports the idea that dimerization serves as a pathway to lower the global electrophilicity of the antiaromatic monomer, achieving a more electronically stable state. Together, these concepts provide a theoretical framework that complements the frontier orbital analysis.

The GEI serves as a valuable descriptor for assessing the electrophilic character of molecular species along a reaction pathway. According to the Minimum Electrophilicity Principle (MEP), chemical systems tend to evolve toward states of lower electrophilicity to achieve greater electronic stability.

As presented in Table 6.2, the GEI values for all pentalene derivatives exhibit consistent trends during the dimerization process. For the unsubstituted pentalene, the GEI slightly decreases from 0.19 in the monomer to 0.18 at the transition state, before increasing to 0.21 in the dimer. This suggests that the transition state is electronically less electrophilic than the reactant, supporting a reactive intermediate that temporarily reduces electrophilic character before stabilizing in the dimeric form.

**Table 6.2**: Calculated GEI values (in atomic units, a.u.) for unsubstituted and substituted pentalene systems.

| **Substituent** | Reactants | | TS | | Dimer | |
|---|---|---|---|---|---|---|
| | int | ext | int | ext | int | ext |
| –H (pentalene) | 0.1921 | — | 0.1817 | — | 0.2171 | — |
| –OH | 0.1858 | 0.1858 | 0.1775 | 0.1775 | 0.2153 | 0.2051 |
| –CN | 0.2287 | 0.2287 | 0.2156 | 0.2170 | 0.2406 | 0.2508 |
| –COOMe | 0.2105 | 0.2105 | 0.1981 | 0.1991 | 0.2233 | 0.2311 |
| –CHO | 0.2196 | 0.2196 | 0.1868 | 0.2077 | 0.2310 | 0.2397 |
| –t-Bu | 0.1839 | 0.1839 | 0.1781 | 0.1739 | 0.2137 | 0.2107 |

In substituted systems, similar patterns are observed. For instance, the –OH derivative shows a slight drop from 0.1858 in the reactant to 0.1775 at the transition state (both interior and exterior), followed by an increase to 0.2153 (interior) and 0.2051 (exterior) in

the dimer. This implies that the dimerization process effectively lowers electrophilicity at the transition state, aligning with the MEP.

The –CN substituent, known for its strong electron-withdrawing nature, shows higher GEI values throughout the process (0.2287 in the monomer, 0.2156–0.2170 at the transition state, and up to 0.2508 in the dimer). This indicates that although the transition state is less electrophilic than the reactant, the final dimer retains a relatively high electrophilicity, potentially due to the persistent electronic effects of the cyano group.

Other substituents, such as –COOMe and –CHO, follow similar trends, with GEI values decreasing at the transition state and rising again in the dimer, though to varying extents depending on their electronic nature. Notably, the tert-butyl group (–t-Bu) maintains the lowest GEI values among all substituents, reflecting its electron-donating and sterically bulky character that favors lower electrophilicity.

Overall, these observations confirm that the dimerization pathway of pentalene derivatives consistently involves a reduction in electrophilicity at the transition state, which supports the principle that systems minimize their electrophilic character during the critical point of reactivity. The final increase in GEI observed in dimers indicates the establishment of a new electronic configuration that is more stable than the initial antiaromatic monomers. This analysis underscores how substituent effects modulate electrophilicity and shape the balance between reactivity and final electronic stability in these antiaromatic systems.

## 6.3 Bell–Evans–Polanyi relationship and Hammond–Leffler postulate

The Bell–Evans–Polanyi (BEP) relationship and the Hammond–Leffler postulate are two complementary frameworks that connect thermodynamic and geometric aspects of reaction mechanisms. Together, they provide a deeper understanding of how substituent effects modulate both activation barriers and transition state structures during pentalene dimerization.

The BEP relationship was first applied to correlate the Gibbs free energy of activation ($\Delta G^{\ddagger}$) with the reaction Gibbs free energy ($\Delta G_r$) for the different substituted pentalene systems. For the “out” dimerization pathway, the linear regression equation obtained

was: $\Delta G^{\ddagger} = 0.4804 \cdot \Delta G_r + 20.664$ with a coefficient of determination $R^2 = 0.5408$. This moderate positive correlation suggests that, for this configuration, the activation barrier partially depends on the thermodynamic driving force. The slope ($\alpha \approx 0.48$) indicates an intermediate sensitivity of the transition state to the reaction exergonicity: as the reaction becomes more exergonic (more negative $\Delta G_r$), the barrier tends to decrease. However, the correlation is not perfect, suggesting that while the BEP model can qualitatively rationalize trends for "out" dimers, additional factors such as steric effects still play an important role.

In contrast, for the "in" dimerization pathway, the regression yielded: $\Delta G^{\ddagger} = -0.4908 \cdot \Delta G_r + 24.956$ with a very low $R^2 = 0.0364$. The negative slope and poor correlation coefficient indicate that, in this case, the activation barriers are not governed by the thermodynamic favorability predicted by the BEP model. Instead, this suggests that strong steric hindrance among inward-facing substituents and unfavorable electronic interactions dominate, leading to a breakdown of the classical linear free energy relationship. The scattered data distribution supports the conclusion that steric congestion within the cavity overrides the purely thermodynamic effects.

Complementarily, the Hammond–Leffler postulate was employed to assess how the structure of transition states varies with reaction energetics. By analyzing the correlation between $\Delta G^{\ddagger}$ and the forming bond distances, it is possible to infer whether transition states are more reactant-like (early) or product-like (late). For the "out" dimers, the relationship was described by: $y = 0.3804x + 21.014$ with $R^2 = 0.3392$, suggesting that as barriers increase, the transition state geometry becomes slightly more reactant-like (longer forming bonds). Although this moderate correlation confirms the general applicability of the Hammond–Leffler postulate, it also highlights the influence of substituent-induced steric and electronic effects.

For the "in" dimers, the stronger slope observed, $y = 1.3382x + 18.554$ with $R^2 = 0.2708$, indicates a steeper dependence of bond distance on activation barrier, albeit with a lower correlation. This suggests that steric congestion inside the dimer cavity more strongly affects the transition state geometry, leading to more reactant-like structures at higher barriers. The tert-butyl group, for example, displays the highest barrier (31.80 kcal/mol) and the longest forming bond distance (2.41 Å), confirming a pronounced early transition state. Conversely, substituents such as –CHO and –OH exhibit lower barriers and shorter forming bonds, corresponding to more product-like transition states.

Overall, these combined analyses reveal that while the BEP relationship partially explains the "out" dimerization pathway, it breaks down in the "in" case due to strong steric effects. The Hammond–Leffler postulate generally holds for both pathways, though with limited predictive precision due to substituent-specific steric and electronic contributions. Together, these frameworks offer a powerful interpretative lens, illustrating how pentalene's intrinsic antiaromatic instability and substituent effects interplay to shape both the kinetics and structural evolution of its dimerization process.

## 6.4 Aromaticity indices and (anti)aromatic character

To understand the role of (anti)aromatic character in driving the dimerization of pentalene, I evaluated aromaticity changes along the reaction using the multicenter index (MCI) and the $I_{ring}$ index. These were computed with the ESIpy program using the IAO (Intrinsic Atomic Orbital) partitioning scheme, which was selected following consultation with the program's author. This scheme provides a balanced description of delocalization effects, avoiding the known artifacts of Mulliken or Löwdin partitions.

For the unsubstituted pentalene (Figure 6.1), the calculated normalized MCI and $I_{ring}$ values in the monomer (reactant) state are approximately 0.506 and 0.504, respectively. These values reflect a notable level of $\pi$-electron delocalization within the two five-membered rings, yet also hint at the destabilizing antiaromatic character intrinsic to the $8\pi$ system.

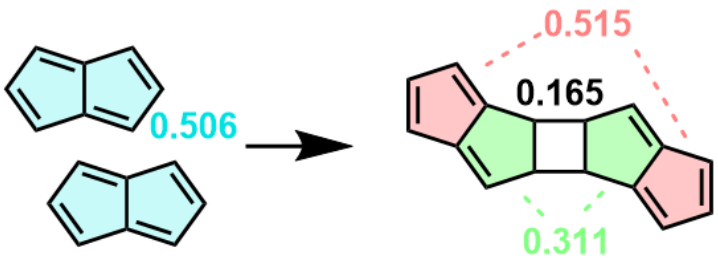


**Figure 6.1**: Normalized MCI values calculated for the unsubstituted pentalene dimerization process (for each ring).

Upon dimerization, a substantial reduction in these aromaticity indices is observed. In the final dimeric product, normalized MCI values decrease to approximately 0.311 for the inward ring, and increases up to 0.362 for the outward ring, while $I_{ring}$ values similarly drop to around 0.316 for the inner and rises up to 0.510 for the outter, respectively. This decline in delocalization indexes highlights the pronounced relief of antiaromatic strain upon forming $\sigma$ bonds in the dimer, which transforms the $\pi$ system into a more localized and energetically stabilized framework.

This marked reduction in aromaticity indices for the inward rings after dimerization supports the idea that the driving force behind the reaction is not only geometric strain relief but also the electronic stabilization achieved by reducing antiaromaticity. The transition from a delocalized, high-energy $\pi$ system to a more $\sigma$-bonded, localized arrangement is consistent with the observed strong thermodynamic preference for dimer formation.

While this section explicitly details the case of unsubstituted pentalene, it is important to note that all studied substituents (regardless of electronic nature or whether oriented inward or outward) follow the same qualitative trend (Appendix A). In each case, the transition from monomer to dimer is accompanied by a clear decrease in both MCI and $I_{ring}$ values for the rings that involve the formation of the new $\sigma$ bonds, underscoring the general tendency of pentalene derivatives to reduce antiaromatic character upon dimerization as a fundamental stabilizing mechanism.

# Chapter 7

# Conclusions

In this thesis, a detailed computational investigation of the dimerization of pentalene and its substituted derivatives was carried out using DFT methods. The findings confirm that the pronounced antiaromatic character of pentalene strongly predisposes it to undergo spontaneous [2+2] cycloaddition, resulting in dimeric products that alleviate the electronic instability of the monomer. The dimerization proceeds via an asynchronous concerted mechanism, with low activation barriers consistent with the Bell–Evans–Polanyi relationship and Hammond–Leffler postulate, indicating early transition states for highly exergonic reactions.

The introduction of electron-donating and electron-withdrawing substituents at strategic positions significantly impacts both the thermodynamics and kinetics of the dimerization process. Electron-withdrawing groups, such as -–CN and -–COOMe, tend to stabilize the monomeric form by reducing its electrophilicity and increasing activation barriers, whereas bulky groups such as —t-Bu introduce strong steric hindrance, especially in inward-oriented transition states, thereby suppressing dimer formation. Conversely, hydroxyl and formyl substituents strike a balance between moderate electronic stabilization and manageable steric effects, enabling relatively favorable dimerization pathways.

Analysis of HOMO–LUMO gaps, and aromaticity indices (MCI and Iring) provides further support for the observed reactivity trends. The evolution of these descriptors along the reaction coordinate aligns with the Maximum Hardness and Minimum Electrophilicity principles, emphasizing the intrinsic drive of antiaromatic systems to achieve greater electronic stability through dimerization.

Overall, this work offers a mechanistic framework for understanding and predicting the reactivity of antiaromatic systems, particularly pentalene derivatives. The insights gained here can guide the rational design of stable, functional antiaromatic compounds for use in optoelectronic and molecular materials applications, where control over electronic properties and structural persistence is critical.

# Bibliography


[1] Israel Fernandez, ed. *Aromaticity*. Elsevier Science Publishing, 2021.

[2] Miquel Solà. "Aromaticity rules". In: *Nat. Chem.* 14 (2022), pp. 585–590.

[3] Miquel Solà et al. *Aromaticity and Antiaromaticity: Concepts and Applications*. Nashville, TN: John Wiley & Sons, 2022.

[4] W von E. Doering and Francis L Detert. "Cycloheptatrienylium oxide". In: *J. Am. Chem. Soc.* 73 (1951), pp. 876–877.

[5] Erich Hückel. "Quantentheoretische Beiträge zum Benzolproblem". In: *Eur. Phys. J. A* 70 (1931), pp. 204–286.

[6] Ronald Breslow. "Antiaromaticity". In: *Acc. Chem. Res.* 6 (1973), pp. 393–398.

[7] A W Hofmann. "I. On insolinic acid". In: *Proc. R. Soc. Lond.* 8 (1857), pp. 1–3.

[8] Miquel Solà. "Why Aromaticity Is a Suspicious Concept? Why?" In: *Frontiers in Chemistry* 5 (2017), p. 22.

[9] Michał Ksawery Cyrański. "Energetic Aspects of Cyclic Pi-Electron Delocalization: Evaluation of the Methods of Estimating Aromatic Stabilization Energies". In: *Chemical Reviews* 105 (2005), pp. 3773–3811.

[10] T M Krygowski and M K Cyrański. "Structural aspects of aromaticity". In: *Chem. Rev.* 101 (2001), pp. 1385–1419.

[11] Zhongfang Chen et al. "Nucleus-independent chemical shifts (NICS) as an aromaticity criterion". In: *Chem. Rev.* 105 (2005), pp. 3842–3888.

[12] Daniel Geuenich et al. "Anisotropy of the induced current density (ACID), a general method to quantify and visualize electronic delocalization". In: *Chem. Rev.* 105 (2005), pp. 3758–3772.

[13] Heike Fliegl et al. “The gauge including magnetically induced current method”. In: *Phys. Chem. Chem. Phys.* 13 (2011), pp. 20500–20518.

[14] Jordi Poater et al. “Theoretical evaluation of electron delocalization in aromatic molecules by means of atoms in molecules (AIM) and electron localization function (ELF) topological approaches”. In: *Chem. Rev.* 105 (2005), pp. 3911–3947.

[15] Ferran Feixas et al. “Quantifying aromaticity with electron delocalisation measures”. In: *Chem. Soc. Rev.* 44 (2015), pp. 6434–6451.

[16] Gabriel Merino et al. “Aromaticity: Quo Vadis”. In: *Chem. Sci.* 14 (2023), pp. 5569–5576.

[17] P Lazzeretti. “Ring currents”. In: *Prog. Nucl. Magn. Reson. Spectrosc.* 36 (2000), pp. 1–88.

[18] Abraham Minsky, Amatzya Y Meyer, and Mordecai Rabinovitz. “Paratropicity and antiaromaticity: role of the HOMO-LUMO energy gap”. In: *Tetrahedron* 41 (1985), pp. 785–791.

[19] Ralph G Pearson. “Recent advances in the concept of hard and soft acids and bases”. In: *J. Chem. Educ.* 64 (1987), p. 561.

[20] Lucas José Karas and Judy I-Chia Wu. “Antiaromatic compounds: a brief history, applications, and the many ways they escape antiaromaticity”. In: *Aromaticity*. Elsevier, 2021, pp. 319–338.

[21] N Colin Baird. “Quantum organic photochemistry. II. Resonance and aromaticity in the lowest 3.pi..pi.* state of cyclic hydrocarbons”. In: *J. Am. Chem. Soc.* 94 (1972), pp. 4941–4948.

[22] Henrik Ottosson. “Organic photochemistry: Exciting excited-state aromaticity”. In: *Nat. Chem.* 4 (2012), pp. 969–971.

[23] Martin Rosenberg et al. “Excited state aromaticity and antiaromaticity: opportunities for photophysical and photochemical rationalizations”. In: *Chem. Rev.* 114 (2014), pp. 5379–5425.

[24] Raffaello Papadakis and Henrik Ottosson. “The excited state antiaromatic benzene ring: a molecular Mr Hyde?” In: *Chem. Soc. Rev.* 44 (2015), pp. 6472–6493.

[25] Jinseok Kim et al. “Porphyrinoids, a unique platform for exploring excited-state aromaticity”. In: *Chem. Soc. Rev.* 51 (2022), pp. 268–292.

[26] Jiajie Yan et al. “Photochemistry driven by excited-state aromaticity gain or antiaromaticity relief”. In: *Chemistry* 29 (2023), e202203748.

[27] Florian Glöcklhofer. “Concealed antiaromaticity”. In: *Open Res. Eur.* 5 (2025), p. 70.

[28] Wojciech Stawski et al. “Crystallographic evidence for global aromaticity in the di-anion and tetra-anion of a cyclophane hydrocarbon”. In: *Chem. Sci.* 14 (2023), pp. 14109–14114.

[29] Wojciech Stawski et al. “The anti-aromatic dianion and aromatic tetraanion of [18]annulene”. In: *Nat. Chem.* 16 (2024), pp. 998–1002.

[30] Tullimilli Y Gopalakrishna and Venkataramanarao G Anand. “Reversible redox reaction between antiaromatic and aromatic states of 32$\pi$-expanded isophlorins”. In: *Angew. Chem. Int. Ed Engl.* 53 (2014), pp. 6678–6682.

[31] Simon Eder et al. “Switching between local and global aromaticity in a conjugated macrocycle for high-performance organic sodium-ion battery anodes”. In: *Angew. Chem. Int. Ed Engl.* 59 (2020), pp. 12958–12964.

[32] Won-Young Cha et al. “Multifaceted [36]octaphyrin(1.1.1.1.1.1.1.1): deprotonation-induced switching among nonaromatic, Möbius aromatic, and Hückel antiaromatic species”. In: *Chem. Commun. (Camb.)* 52 (2016), pp. 6076–6078.

[33] Tullimilli Y Gopalakrishna, J Sreedhar Reddy, and Venkataramanarao G Anand. “An amphoteric switch to aromatic and antiaromatic states of a neutral air-stable 25$\pi$ radical”. In: *Angew. Chem. Int. Ed Engl.* 53 (2014), pp. 10984–10987.

[34] Yikun Zhu et al. “What a difference an electron makes: Structural response of saddle-shaped tetraphenylene to one and two electron uptake”. In: *ChemistryEurope* 2 (2024).

[35] Xiaodong Yin et al. “A reversible single-molecule switch based on activated antiaromaticity”. In: *Sci. Adv.* 3 (2017), eaao2615.

[36] Hugh J Sanderson et al. “Reversible formation of tetraphenylpentalene, a room temperature stable antiaromatic hydrocarbon”. In: *Chem. Sci.* 16 (2025), pp. 952–961.

[37] Thomas Bally et al. “Pentalene: Formation, electronic, and vibrational structure”. In: *J. Am. Chem. Soc.* 119 (1997), pp. 1869–1875.

[38] Marija Baranac-Stojanović. “A DFT study of the modulation of the antiaromatic and open-shell character of dibenzo[a,f]pentalene by employing three strategies: Additional benzoannulation, BN/CC isosterism, and substitution”. In: *Chemistry* 25 (2019), pp. 9747–9757.

[39] Andrew E Ashley, Andrew R Cowley, and Dermot O'Hare. "Permethylpentalene chemistry". In: *European J. Org. Chem.* 2007 (2007), pp. 2239–2242.

[40] Klaus Hartke and Rudolf Matusch. "Aminopentalenecarbonitriles, a Group of Stable Pentalenes". In: *Angew. Chem. Int. Ed. Engl.* 11 (1972), pp. 50–51.

[41] Klaus Hafner and Hans Ulrich Süss. "1,3,5-Tri-*tert*-butylpentalene. A stabilized planar 8$\pi$-electron system". In: *Angew. Chem., Int. Ed. Engl.* 12 (1973), pp. 575–577.

[42] Zerubba U Levi and T Don Tilley. "Versatile synthesis of pentalene derivatives via the Pd-catalyzed homocoupling of haloenynes". In: *J. Am. Chem. Soc.* 131 (2009), pp. 2796–2797.

[43] Minoru Suda and Klaus Hafner. "Synthesis of 4.6-di-tert.-butyl-pentalene derivatives and their reversible dimerization". In: *Tetrahedron Lett.* 18 (1977), pp. 2449–2452.

[44] Paul von Ragué Schleyer et al. "Nucleus-independent chemical shifts: A simple and efficient aromaticity probe". In: *J. Am. Chem. Soc.* 118 (1996), pp. 6317–6318.

[45] J. Kruszewski and T.M. Krygowski. "Definition of aromaticity basing on the harmonic oscillator model". In: *Tetrahedron Letters* 13 (1972), pp. 3839–3842.

[46] Zachary W Schroeder et al. "Sterically hindered derivatives of pentacene and octafluoropentacene". In: *Chemistry* 30 (2024), e202402651.

[47] Masahiro Nakano et al. "Novel dibenzo[a,e]pentalene-based conjugated polymers". In: *J. Mater. Chem. C Mater. Opt. Electron. Devices* 2 (2014), pp. 64–70.

[48] Akihito Konishi et al. "Enhancement of Antiaromatic Character via Additional Benzoannulation into Dibenzo[ a, f]pentalene: Syntheses and Properties of Benzo[ a]naphtho[2,1- f]pentalene and Dinaphtho[2,1- a, f]pentalene". In: *J. Am. Chem. Soc.* 141 (2019), pp. 560–571.

[49] Jianglin Wu et al. "Tuning the antiaromatic character and charge transport of pentalene-based antiaromatic compounds by substitution". In: *J. Mater. Chem. C Mater. Opt. Electron. Devices* 10 (2022), pp. 2724–2731.

[50] Mina Ahn et al. "Systematic radical species control by electron push-pull substitution in the perylene-based D-$\pi$-A compounds". In: *RSC Adv.* 13 (2023), pp. 2283–2293.

[51] Henning Hopf. "Pentalenes–from highly reactive antiaromatics to substrates for material science". In: *Angew. Chem. Int. Ed Engl.* 52 (2013), pp. 12224–12226.

[52] William P Jencks. “A primer for the Bema Hapothle. An empirical approach to the characterization of changing transition-state structures”. In: *Chem. Rev.* 85 (1985), pp. 511–527.

[53] George S Hammond. “A correlation of reaction rates”. In: *J. Am. Chem. Soc.* 77 (1955), pp. 334–338.

[54] Addy Pross. *Theoretical and physical principles of organic reactivity*. John Wiley & Sons, 1995.

[55] Miquel Solà and Alejandro Toro-Labbé. “The Hammond postulate and the principle of maximum hardness in some intramolecular rearrangement reactions”. In: *J. Phys. Chem. A* 103 (1999), pp. 8847–8852.

[56] Robert G Parr, László v Szentpály, and Shubin Liu. “Electrophilicity index”. In: *J. Am. Chem. Soc.* 121 (1999), pp. 1922–1924.

[57] Pratim Kumar Chattaraj, Utpal Sarkar, and Debesh Ranjan Roy. “Electrophilicity index”. In: *Chem. Rev.* 106 (2006), pp. 2065–2091.

[58] Eduardo Chamorro, Pratim K Chattaraj, and Patricio Fuentealba. “Variation of the electrophilicity index along the reaction path”. In: *J. Phys. Chem. A* 107 (2003), pp. 7068–7072.

[59] Bingxin Yuan et al. “Pentaleno[1,2-a:4,5′]diacenaphthylenes: Uniquely stabilized pentalene derivatives”. In: *J. Org. Chem.* 81 (2016), pp. 8312–8318.

[60] Yuanchen Shen et al. “Heteroatom-doping engineering of fused Olympic cations: Metal-free modular syntheses and NIR-II radicals with mixed aromatic/antiaromatic characters”. In: *Angew. Chem. Int. Ed Engl.* 64 (2025), e202503989.

[61] M. J. Frisch et al. *Gaussian~16 Revision C.01*. Gaussian Inc. Wallingford CT. 2016.

[62] Axel D Becke. “Density-functional thermochemistry. III. The role of exact exchange”. In: *J. Chem. Phys.* 98 (1993), pp. 5648–5652.

[63] C Lee, W Yang, and R G Parr. “Development of the Colle-Salvetti correlation-energy formula into a functional of the electron density”. In: *Phys. Rev. B Condens. Matter* 37 (1988), pp. 785–789.

[64] S H Vosko, L Wilk, and M Nusair. “Accurate spin-dependent electron liquid correlation energies for local spin density calculations: a critical analysis”. In: *Can. J. Phys.* 58 (1980), pp. 1200–1211.

[65] P J Stephens et al. “Ab initio calculation of vibrational absorption and circular dichroism spectra using density functional force fields”. In: *J. Phys. Chem.* 98 (1994), pp. 11623–11627.

[66] Stefan Grimme, Stephan Ehrlich, and Lars Goerigk. “Effect of the damping function in dispersion corrected density functional theory”. In: *J. Comput. Chem.* 32 (2011), pp. 1456–1465.

[67] Carlos Gonzalez and H Bernhard Schlegel. “An improved algorithm for reaction path following”. In: *J. Chem. Phys.* 90 (1989), pp. 2154–2161.

[68] Patrick Bultinck, Robert Ponec, and Sofie Van Damme. “Multicenter bond indices as a new measure of aromaticity in polycyclic aromatic hydrocarbons”. In: *Journal of Physical Organic Chemistry* 18 (2005), pp. 706–718.

[69] Mario Giambiagi, Myriam S. De Giambiagi, and Kleber C. Mundim. “Definition of a multicenter bond index”. In: *Structural Chemistry* 1 (1990), pp. 423–427.

[70] Joan Grèbol-Tomàs, Eduard Matito, and Pedro Salvador. “Can Aromaticity Be Evaluated Using Atomic Partitions Based on the Hilbert-Space?” In: *Chem. Eur. J.* 30 (2024), e202401282.

[71] Yi Li and K N Houk. “The dimerization of cyclobutadiene. An ab initio CASSCF theoretical study”. In: *J. Am. Chem. Soc.* 118 (1996), pp. 880–885.

[72] R B Woodward and Roald Hoffmann. “Stereochemistry of electrocyclic reactions”. In: *J. Am. Chem. Soc.* 87 (1965), pp. 395–397.

[73] Mesías Orozco-Ic and Dage Sundholm. “On the antiaromatic-aromatic-antiaromatic transition of the stacked cyclobutadiene dimer”. In: *Phys. Chem. Chem. Phys.* 25 (2023), pp. 12777–12782.

# Appendix

# Appendix A

# Aromaticity index for all the systems

In this appendix, I present a comprehensive set of numerical results for the aromaticity analysis performed on pentalene and its substituted derivatives. The evaluation of aromaticity was carried out using multicenter indices, specifically the multicenter index (MCI) and $I_{ring}$, which provide a quantitative measure of electron delocalization within each ring. Calculations were conducted with the ESIpy program using different population analysis schemes, including Mulliken, Löwdin, Metalöwdin, NAO, and IAO partitions. The tables summarize, for each ring in the system, the raw and normalized values of MCI and $I_{ring}$, facilitating direct comparisons between different substituents, conformations, and partitions. The ring distribution follows the numbering of Figure A.1:

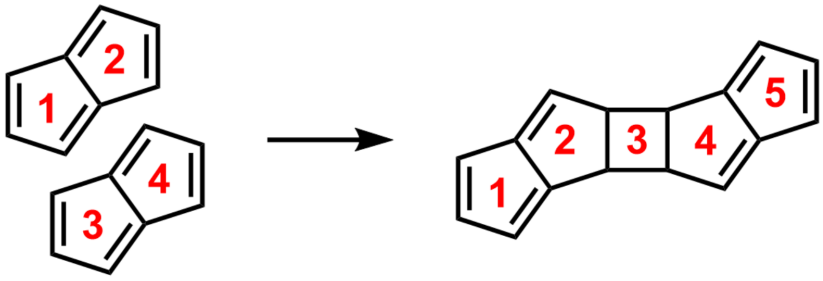


**Figure A.1**: Schematic representation of the unsubstituted pentalene dimerization, with rings numbered for the analysis of local aromaticity analysis.

**Table A.1**: Aromaticity indices (MCI and $I_{ring}$) for each ring of the pentalene reactant structure, computed using different population analysis partitions.

| Partition | Ring | MCI | $MCI^{1/2}$ | $I_{ring}$ | $I_{ring}{}^{1/2}$ |
|---|---|---|---|---|---|
| Mulliken | 1 | 0.418546 | 0.840134 | 0.337211 | 0.804601 |
| | 2 | 0.421581 | 0.841349 | 0.336720 | 0.804366 |
| | 3 | 0.421386 | 0.841271 | 0.212469 | 0.733600 |
| | 4 | 0.421190 | 0.841193 | 0.211844 | 0.733167 |
| Löwdin | 1 | 0.017160 | 0.443511 | 0.020170 | 0.458080 |
| | 2 | 0.017156 | 0.443489 | 0.020168 | 0.458070 |
| | 3 | 0.017167 | 0.443546 | 0.020175 | 0.458104 |
| | 4 | 0.017184 | 0.443634 | 0.020190 | 0.458172 |
| Metalöwdin | 1 | 0.031712 | 0.501470 | 0.031923 | 0.502135 |
| | 2 | 0.031700 | 0.501433 | 0.031915 | 0.502110 |
| | 3 | 0.031719 | 0.501492 | 0.031930 | 0.502157 |
| | 4 | 0.031747 | 0.501579 | 0.031953 | 0.502231 |
| NAO | 1 | 0.030880 | 0.498809 | 0.030595 | 0.497886 |
| | 2 | 0.030868 | 0.498770 | 0.030587 | 0.497859 |
| | 3 | 0.030886 | 0.498829 | 0.030601 | 0.497907 |
| | 4 | 0.030914 | 0.498919 | 0.030625 | 0.497984 |
| IAO | 1 | 0.033099 | 0.505783 | 0.032667 | 0.504455 |
| | 2 | 0.033086 | 0.505743 | 0.032659 | 0.504429 |
| | 3 | 0.033106 | 0.505801 | 0.032674 | 0.504476 |
| | 4 | 0.033135 | 0.505892 | 0.032699 | 0.504552 |

**Table A.2**: Aromaticity indices (MCI and $I_{ring}$) for each ring of the pentalene dimer structure, computed using different population analysis partitions.

| Partition | Ring | MCI | $MCI^{1/2}$ | $I_{ring}$ | $I_{ring}^{1/2}$ |
|---|---|---|---|---|---|
| Mulliken | 1 | 0.385433 | 0.826399 | 0.160175 | 0.693296 |
| | 2 | 0.520685 | 0.877637 | 0.284247 | 0.777570 |
| | 3 | 0.208594 | 0.675812 | 0.139073 | 0.610676 |
| | 4 | 0.520685 | 0.877637 | 0.283917 | 0.777389 |
| | 5 | 0.385433 | 0.826399 | 0.160175 | 0.693296 |
| Löwdin | 1 | 0.018494 | 0.450200 | 0.021671 | 0.464704 |
| | 2 | 0.000066 | 0.145917 | 0.002849 | 0.309691 |
| | 3 | 0.006350 | 0.282283 | -0.003367 | -0.240892 |
| | 4 | 0.000066 | 0.145917 | 0.002849 | 0.309691 |
| | 5 | 0.018494 | 0.450200 | 0.021671 | 0.464704 |
| Metalöwdin | 1 | 0.034344 | 0.509532 | 0.033651 | 0.507459 |
| | 2 | 0.002691 | 0.306189 | 0.003158 | 0.316144 |
| | 3 | 0.001018 | 0.178604 | 0.000604 | 0.156799 |
| | 4 | 0.002691 | 0.306189 | 0.003158 | 0.316144 |
| | 5 | 0.034344 | 0.509532 | 0.033651 | 0.507459 |
| NAO | 1 | 0.033986 | 0.508464 | 0.032754 | 0.504722 |
| | 2 | 0.001991 | 0.288286 | 0.002171 | 0.293323 |
| | 3 | 0.001013 | 0.178384 | 0.000528 | 0.151591 |
| | 4 | 0.001991 | 0.288286 | 0.002171 | 0.293323 |
| | 5 | 0.033986 | 0.508464 | 0.032754 | 0.504722 |
| IAO | 1 | 0.036110 | 0.514665 | 0.034339 | 0.509517 |
| | 2 | 0.002902 | 0.310839 | 0.003140 | 0.315785 |
| | 3 | 0.000732 | 0.164512 | 0.000455 | 0.146042 |
| | 4 | 0.002902 | 0.310839 | 0.003140 | 0.315785 |
| | 5 | 0.036110 | 0.514665 | 0.034339 | 0.509517 |

**Table A.3**: Aromaticity indices (MCI and $I_{ring}$) for each ring of the aldehyde reactant substituent structure, computed using different population analysis partitions.

| Partition | Ring | MCI | $MCI^{1/2}$ | $I_{ring}$ | $I_{ring}{}^{1/2}$ |
|---|---|---|---|---|---|
| Mulliken | 1 | 0.489146 | 0.866738 | 0.095743 | 0.625492 |
| | 2 | 0.777877 | 0.951004 | 0.248942 | 0.757216 |
| | 3 | 0.777388 | 0.950884 | 0.498690 | 0.870094 |
| | 4 | 0.488617 | 0.866550 | 0.342594 | 0.807153 |
| Löwdin | 1 | 0.017550 | 0.445509 | 0.020579 | 0.459924 |
| | 2 | 0.017448 | 0.444989 | 0.019993 | 0.457272 |
| | 3 | 0.017456 | 0.445032 | 0.019999 | 0.457301 |
| | 4 | 0.017542 | 0.445465 | 0.020572 | 0.459892 |
| Metalöwdin | 1 | 0.032689 | 0.504523 | 0.032762 | 0.504748 |
| | 2 | 0.032111 | 0.502725 | 0.031847 | 0.501895 |
| | 3 | 0.032126 | 0.502773 | 0.031859 | 0.501934 |
| | 4 | 0.032673 | 0.504474 | 0.032749 | 0.504709 |
| NAO | 1 | 0.031779 | 0.501681 | 0.031332 | 0.500262 |
| | 2 | 0.031283 | 0.500107 | 0.030498 | 0.497571 |
| | 3 | 0.031299 | 0.500156 | 0.030510 | 0.497611 |
| | 4 | 0.031763 | 0.501629 | 0.031319 | 0.500220 |
| IAO | 1 | 0.033966 | 0.508405 | 0.033441 | 0.506823 |
| | 2 | 0.033374 | 0.506618 | 0.032573 | 0.504163 |
| | 3 | 0.033390 | 0.506668 | 0.032585 | 0.504201 |
| | 4 | 0.033949 | 0.508352 | 0.033428 | 0.506782 |

**Table A.4**: Aromaticity indices (MCI and $I_{ring}$) for each ring of the aldehyde immer product substituent structure, computed using different population analysis partitions.

| Partition | Ring | MCI | $MCI^{1/2}$ | $I_{ring}$ | $I_{ring}{}^{1/2}$ |
|---|---|---|---|---|---|
| Mulliken | 1 | 0.679450 | 0.925617 | 0.066672 | 0.581821 |
| | 2 | 0.445947 | 0.850857 | 0.231149 | 0.746068 |
| | 3 | 0.300317 | 0.740278 | 0.261951 | 0.715410 |
| | 4 | -1.648644 | -1.105161 | -0.051433 | -0.552394 |
| | 5 | 0.266404 | 0.767553 | 0.107052 | 0.639615 |
| Löwdin | 1 | 0.015910 | 0.436853 | 0.019968 | 0.457159 |
| | 2 | -0.000059 | -0.142700 | 0.002536 | 0.302568 |
| | 3 | 0.006807 | 0.287241 | -0.002515 | -0.223940 |
| | 4 | 0.000045 | 0.135284 | 0.002589 | 0.303823 |
| | 5 | 0.017614 | 0.445833 | 0.020815 | 0.460974 |
| Metalöwdin | 1 | 0.031396 | 0.500467 | 0.031703 | 0.501442 |
| | 2 | 0.002627 | 0.304724 | 0.003045 | 0.313851 |
| | 3 | 0.001191 | 0.185759 | 0.000724 | 0.164040 |
| | 4 | 0.002671 | 0.305721 | 0.003012 | 0.313164 |
| | 5 | 0.033841 | 0.508029 | 0.033044 | 0.505612 |
| NAO | 1 | 0.030998 | 0.499190 | 0.030748 | 0.498382 |
| | 2 | 0.001857 | 0.284299 | 0.001967 | 0.287573 |
| | 3 | 0.001039 | 0.179550 | 0.000531 | 0.151780 |
| | 4 | 0.001920 | 0.286195 | 0.001980 | 0.287969 |
| | 5 | 0.033451 | 0.506854 | 0.032035 | 0.502487 |
| IAO | 1 | 0.033052 | 0.505639 | 0.032377 | 0.503554 |
| | 2 | 0.002818 | 0.309017 | 0.003022 | 0.313366 |
| | 3 | 0.000949 | 0.175525 | 0.000614 | 0.157436 |
| | 4 | 0.002866 | 0.310068 | 0.002992 | 0.312740 |
| | 5 | 0.035565 | 0.513103 | 0.033707 | 0.507626 |

**Table A.5**: Aromaticity indices (MCI and $I_{ring}$) for each ring of the aldehyde outter product substituent structure, computed using different population analysis partitions.

| Partition | Ring | MCI | $MCI^{1/2}$ | $I_{ring}$ | $I_{ring}{}^{1/2}$ |
|---|---|---|---|---|---|
| Mulliken | 1 | 0.222529 | 0.740418 | 0.208166 | 0.730604 |
| | 2 | 0.854549 | 0.969053 | 0.299429 | 0.785704 |
| | 3 | 0.461429 | 0.824188 | 0.182357 | 0.653477 |
| | 4 | 0.807519 | 0.958144 | 0.185341 | 0.713829 |
| | 5 | 0.138640 | 0.673562 | 0.024897 | 0.477781 |
| Löwdin | 1 | 0.018665 | 0.451030 | 0.021038 | 0.461955 |
| | 2 | -0.000020 | -0.114734 | 0.002842 | 0.309554 |
| | 3 | 0.006303 | 0.281761 | -0.003374 | -0.241015 |
| | 4 | -0.000057 | -0.141835 | 0.002834 | 0.309371 |
| | 5 | 0.017736 | 0.446450 | 0.020366 | 0.458965 |
| Metalöwdin | 1 | 0.033975 | 0.508431 | 0.032760 | 0.504741 |
| | 2 | 0.002707 | 0.306549 | 0.003166 | 0.316308 |
| | 3 | 0.001004 | 0.177984 | 0.000583 | 0.155382 |
| | 4 | 0.002711 | 0.306628 | 0.003172 | 0.316419 |
| | 5 | 0.032422 | 0.503697 | 0.031567 | 0.501010 |
| NAO | 1 | 0.033572 | 0.507218 | 0.031913 | 0.502104 |
| | 2 | 0.001997 | 0.288455 | 0.002175 | 0.293413 |
| | 3 | 0.000994 | 0.177583 | 0.000510 | 0.150248 |
| | 4 | 0.002005 | 0.288671 | 0.002183 | 0.293637 |
| | 5 | 0.031973 | 0.502292 | 0.030702 | 0.498233 |
| IAO | 1 | 0.035537 | 0.513022 | 0.033445 | 0.506835 |
| | 2 | 0.002913 | 0.311079 | 0.003145 | 0.315881 |
| | 3 | 0.000717 | 0.163653 | 0.000431 | 0.144124 |
| | 4 | 0.002911 | 0.311035 | 0.003146 | 0.315903 |
| | 5 | 0.033960 | 0.508387 | 0.032208 | 0.503029 |

**Table A.6**: Aromaticity indices (MCI and $I_{ring}$) for each ring of the cyano reactant substituent structure, computed using different population analysis partitions.

| Partition | Ring | MCI | $MCI^{1/2}$ | $I_{ring}$ | $I_{ring}^{1/2}$ |
|---|---|---|---|---|---|
| Mulliken | 1 | 0.351211 | 0.811173 | 0.296042 | 0.783918 |
| | 2 | 0.648426 | 0.917006 | 0.605309 | 0.904472 |
| | 3 | 0.643713 | 0.915669 | 0.349912 | 0.810572 |
| | 4 | 0.356100 | 0.813419 | 0.093640 | 0.622719 |
| Löwdin | 1 | 0.016025 | 0.437480 | 0.019520 | 0.455088 |
| | 2 | 0.016557 | 0.440350 | 0.019098 | 0.453106 |
| | 3 | 0.016544 | 0.440281 | 0.019087 | 0.453050 |
| | 4 | 0.016022 | 0.437464 | 0.019519 | 0.455084 |
| Metalöwdin | 1 | 0.030515 | 0.497627 | 0.031181 | 0.499779 |
| | 2 | 0.031187 | 0.499799 | 0.030660 | 0.498096 |
| | 3 | 0.031162 | 0.499719 | 0.030635 | 0.498016 |
| | 4 | 0.030516 | 0.497629 | 0.031186 | 0.499795 |
| NAO | 1 | 0.029687 | 0.494897 | 0.029828 | 0.495366 |
| | 2 | 0.030243 | 0.496734 | 0.029222 | 0.493334 |
| | 3 | 0.030218 | 0.496652 | 0.029197 | 0.493251 |
| | 4 | 0.029688 | 0.494898 | 0.029833 | 0.495383 |
| IAO | 1 | 0.031725 | 0.501509 | 0.031798 | 0.501742 |
| | 2 | 0.032461 | 0.503817 | 0.031350 | 0.500320 |
| | 3 | 0.032435 | 0.503735 | 0.031324 | 0.500237 |
| | 4 | 0.031726 | 0.501514 | 0.031804 | 0.501759 |

**Table A.7**: Aromaticity indices (MCI and $I_{ring}$) for each ring of the cyano inner product substituent structure, computed using different population analysis partitions.

| Partition | Ring | MCI | $MCI^{1/2}$ | $I_{ring}$ | $I_{ring}{}^{1/2}$ |
|---|---|---|---|---|---|
| Mulliken | 1 | 0.387632 | 0.827340 | 0.144447 | 0.679112 |
| | 2 | 0.171070 | 0.702482 | 0.175101 | 0.705761 |
| | 3 | -0.043789 | -0.457447 | 0.016184 | 0.356676 |
| | 4 | 0.170683 | 0.702163 | 0.187630 | 0.715584 |
| | 5 | 0.387669 | 0.827356 | 0.144489 | 0.679152 |
| Löwdin | 1 | 0.014639 | 0.429637 | 0.019163 | 0.453411 |
| | 2 | -0.000052 | -0.139166 | 0.002563 | 0.303215 |
| | 3 | 0.005996 | 0.278270 | -0.002493 | -0.223443 |
| | 4 | -0.000052 | -0.139154 | 0.002563 | 0.303215 |
| | 5 | 0.014639 | 0.429639 | 0.019163 | 0.453412 |
| Metalöwdin | 1 | 0.029698 | 0.494932 | 0.030449 | 0.497409 |
| | 2 | 0.002609 | 0.304292 | 0.002926 | 0.311348 |
| | 3 | 0.001032 | 0.179222 | 0.000616 | 0.157555 |
| | 4 | 0.002609 | 0.304291 | 0.002926 | 0.311348 |
| | 5 | 0.029699 | 0.494934 | 0.030449 | 0.497410 |
| NAO | 1 | 0.029337 | 0.493722 | 0.029490 | 0.494238 |
| | 2 | 0.001817 | 0.283070 | 0.001868 | 0.284620 |
| | 3 | 0.000964 | 0.176202 | 0.000460 | 0.146429 |
| | 4 | 0.001817 | 0.283071 | 0.001868 | 0.284620 |
| | 5 | 0.029337 | 0.493723 | 0.029491 | 0.494239 |
| IAO | 1 | 0.031264 | 0.500046 | 0.031065 | 0.499407 |
| | 2 | 0.002806 | 0.308749 | 0.002903 | 0.310860 |
| | 3 | 0.000830 | 0.169713 | 0.000501 | 0.149598 |
| | 4 | 0.002806 | 0.308749 | 0.002903 | 0.310860 |
| | 5 | 0.031265 | 0.500047 | 0.031066 | 0.499409 |

**Table A.8**: Aromaticity indices (MCI and $I_{ring}$) for each ring of the cyano outter product substituent structure, computed using different population analysis partitions.

| Partition | Ring | MCI | $MCI^{1/2}$ | $I_{ring}$ | $I_{ring}^{1/2}$ |
|---|---|---|---|---|---|
| Mulliken | 1 | 0.396283 | 0.831000 | 0.296004 | 0.783898 |
| | 2 | 0.787609 | 0.953371 | 0.309139 | 0.790734 |
| | 3 | 0.504829 | 0.842920 | 0.220684 | 0.685398 |
| | 4 | 0.787618 | 0.953374 | 0.212460 | 0.733593 |
| | 5 | 0.396275 | 0.830997 | 0.295999 | 0.783895 |
| Löwdin | 1 | 0.018487 | 0.450165 | 0.020906 | 0.461374 |
| | 2 | 0.000006 | 0.091241 | 0.002846 | 0.309633 |
| | 3 | 0.006331 | 0.282080 | -0.003357 | -0.240712 |
| | 4 | 0.000006 | 0.091286 | 0.002846 | 0.309633 |
| | 5 | 0.018487 | 0.450166 | 0.020906 | 0.461375 |
| Metalöwdin | 1 | 0.034153 | 0.508962 | 0.032783 | 0.504813 |
| | 2 | 0.002711 | 0.306643 | 0.003177 | 0.316517 |
| | 3 | 0.001022 | 0.178785 | 0.000601 | 0.156544 |
| | 4 | 0.002711 | 0.306643 | 0.003177 | 0.316517 |
| | 5 | 0.034153 | 0.508963 | 0.032784 | 0.504814 |
| NAO | 1 | 0.033654 | 0.507467 | 0.031867 | 0.501960 |
| | 2 | 0.001999 | 0.288508 | 0.002181 | 0.293574 |
| | 3 | 0.001009 | 0.178231 | 0.000525 | 0.151401 |
| | 4 | 0.001999 | 0.288509 | 0.002181 | 0.293574 |
| | 5 | 0.033654 | 0.507468 | 0.031868 | 0.501961 |
| IAO | 1 | 0.035800 | 0.513779 | 0.033511 | 0.507036 |
| | 2 | 0.002915 | 0.311118 | 0.003153 | 0.316049 |
| | 3 | 0.000737 | 0.164771 | 0.000451 | 0.145724 |
| | 4 | 0.002915 | 0.311118 | 0.003153 | 0.316049 |
| | 5 | 0.035800 | 0.513780 | 0.033512 | 0.507036 |

**Table A.9**: Aromaticity indices (MCI and $I_{ring}$) for each ring of the methyl carboxilate reactant substituent structure, computed using different population analysis partitions.

| Partition | Ring | MCI | $MCI^{1/2}$ | $I_{ring}$ | $I_{ring}{}^{1/2}$ |
|---|---|---|---|---|---|
| Mulliken | 1 | 0.395051 | 0.830483 | 0.123386 | 0.658042 |
| | 2 | 0.626497 | 0.910718 | 0.300883 | 0.786465 |
| | 3 | 0.629728 | 0.911655 | -0.229688 | -0.745123 |
| | 4 | 0.394341 | 0.830184 | 0.331525 | 0.801869 |
| Löwdin | 1 | 0.017560 | 0.445557 | 0.020630 | 0.460151 |
| | 2 | 0.016794 | 0.441604 | 0.019296 | 0.454040 |
| | 3 | 0.016790 | 0.441583 | 0.019294 | 0.454028 |
| | 4 | 0.017567 | 0.445595 | 0.020635 | 0.460172 |
| Metalöwdin | 1 | 0.033170 | 0.505999 | 0.033124 | 0.505858 |
| | 2 | 0.030980 | 0.499132 | 0.030825 | 0.498634 |
| | 3 | 0.030971 | 0.499105 | 0.030820 | 0.498617 |
| | 4 | 0.033181 | 0.506032 | 0.033132 | 0.505882 |
| NAO | 1 | 0.032285 | 0.503268 | 0.031694 | 0.501413 |
| | 2 | 0.030035 | 0.496050 | 0.029362 | 0.493806 |
| | 3 | 0.030027 | 0.496024 | 0.029356 | 0.493788 |
| | 4 | 0.032295 | 0.503302 | 0.031702 | 0.501439 |
| IAO | 1 | 0.034481 | 0.509937 | 0.033800 | 0.507907 |
| | 2 | 0.032185 | 0.502956 | 0.031476 | 0.500722 |
| | 3 | 0.032176 | 0.502928 | 0.031471 | 0.500704 |
| | 4 | 0.034493 | 0.509971 | 0.033809 | 0.507932 |

**Table A.10**: Aromaticity indices (MCI and $I_{ring}$) for each ring of the methyl carboxilate inner product substituent structure, computed using different population analysis partitions.

| Partition | Ring | MCI | $MCI^{1/2}$ | $I_{ring}$ | $I_{ring}^{1/2}$ |
|---|---|---|---|---|---|
| Mulliken | 1 | 0.262418 | 0.765242 | 0.187420 | 0.715424 |
| | 2 | 0.881308 | 0.975047 | 0.311656 | 0.792018 |
| | 3 | 0.318751 | 0.751386 | 0.284160 | 0.730114 |
| | 4 | 0.769648 | 0.948983 | 0.353072 | 0.812031 |
| | 5 | 0.330879 | 0.801556 | 0.230314 | 0.745528 |
| Löwdin | 1 | 0.017339 | 0.444433 | 0.020591 | 0.459975 |
| | 2 | 0.000166 | 0.175310 | 0.002574 | 0.303471 |
| | 3 | 0.006435 | 0.283226 | -0.002516 | -0.223957 |
| | 4 | 0.000035 | 0.128382 | 0.002502 | 0.301764 |
| | 5 | 0.016451 | 0.439781 | 0.019893 | 0.456814 |
| Metalöwdin | 1 | 0.033745 | 0.507739 | 0.033055 | 0.505648 |
| | 2 | 0.002693 | 0.306224 | 0.003061 | 0.314178 |
| | 3 | 0.001237 | 0.187524 | 0.000769 | 0.166515 |
| | 4 | 0.002674 | 0.305808 | 0.003045 | 0.313851 |
| | 5 | 0.032914 | 0.505213 | 0.032570 | 0.504155 |
| NAO | 1 | 0.033312 | 0.506429 | 0.032012 | 0.502414 |
| | 2 | 0.001923 | 0.286280 | 0.002000 | 0.288530 |
| | 3 | 0.001110 | 0.182517 | 0.000586 | 0.155564 |
| | 4 | 0.001886 | 0.285181 | 0.001960 | 0.287383 |
| | 5 | 0.032451 | 0.503785 | 0.031492 | 0.500771 |
| IAO | 1 | 0.035445 | 0.512755 | 0.033724 | 0.507678 |
| | 2 | 0.002884 | 0.310455 | 0.003045 | 0.313838 |
| | 3 | 0.001017 | 0.178569 | 0.000662 | 0.160434 |
| | 4 | 0.002863 | 0.309996 | 0.003026 | 0.313464 |
| | 5 | 0.034619 | 0.510343 | 0.033277 | 0.506324 |

**Table A.11**: Aromaticity indices (MCI and $I_{ring}$) for each ring of the methyl carboxilate outter product substituent structure, computed using different population analysis partitions.

| Partition | Ring | MCI | $MCI^{1/2}$ | $I_{ring}$ | $I_{ring}^{1/2}$ |
|---|---|---|---|---|---|
| Mulliken | 1 | 0.057103 | 0.564068 | 0.012585 | 0.416844 |
| | 2 | 0.782476 | 0.952126 | 0.230494 | 0.745644 |
| | 3 | 0.603866 | 0.881526 | 0.191992 | 0.661943 |
| | 4 | 0.753882 | 0.945063 | 0.131665 | 0.666644 |
| | 5 | 0.088702 | 0.616008 | 0.001837 | 0.283688 |
| Löwdin | 1 | 0.018116 | 0.448347 | 0.020598 | 0.460008 |
| | 2 | -0.000027 | -0.121554 | 0.002834 | 0.309380 |
| | 3 | 0.006297 | 0.281695 | -0.003390 | -0.241296 |
| | 4 | -0.000037 | -0.129720 | 0.002832 | 0.309321 |
| | 5 | 0.017943 | 0.447487 | 0.020536 | 0.459730 |
| Metalöwdin | 1 | 0.033279 | 0.506331 | 0.032237 | 0.503120 |
| | 2 | 0.002705 | 0.306499 | 0.003164 | 0.316254 |
| | 3 | 0.001000 | 0.177817 | 0.000580 | 0.155215 |
| | 4 | 0.002704 | 0.306468 | 0.003163 | 0.316252 |
| | 5 | 0.033056 | 0.505649 | 0.032114 | 0.502736 |
| NAO | 1 | 0.032721 | 0.504620 | 0.031286 | 0.500115 |
| | 2 | 0.001998 | 0.288486 | 0.002173 | 0.293364 |
| | 3 | 0.000993 | 0.177534 | 0.000508 | 0.150109 |
| | 4 | 0.001999 | 0.288503 | 0.002174 | 0.293398 |
| | 5 | 0.032516 | 0.503987 | 0.031179 | 0.499774 |
| IAO | 1 | 0.034826 | 0.510953 | 0.032899 | 0.505168 |
| | 2 | 0.002910 | 0.311008 | 0.003141 | 0.315792 |
| | 3 | 0.000712 | 0.163376 | 0.000428 | 0.143859 |
| | 4 | 0.002907 | 0.310952 | 0.003140 | 0.315775 |
| | 5 | 0.034601 | 0.510291 | 0.032770 | 0.504773 |

**Table A.12**: Aromaticity indices (MCI and $I_{ring}$) for each ring of the alcohol reactant substituent structure, computed using different population analysis partitions.

| Partition | Ring | MCI | $MCI^{1/2}$ | $I_{ring}$ | $I_{ring}^{1/2}$ |
|---|---|---|---|---|---|
| Mulliken | 1 | 0.783264 | 0.952317 | 0.374730 | 0.821758 |
| | 2 | 0.651391 | 0.917843 | 0.184345 | 0.713060 |
| | 3 | 0.650003 | 0.917451 | 0.549319 | 0.887084 |
| | 4 | 0.781783 | 0.951957 | 0.367956 | 0.818765 |
| Löwdin | 1 | 0.017010 | 0.442731 | 0.020228 | 0.458342 |
| | 2 | 0.015584 | 0.435046 | 0.019200 | 0.453589 |
| | 3 | 0.015567 | 0.434952 | 0.019185 | 0.453517 |
| | 4 | 0.017013 | 0.442748 | 0.020234 | 0.458371 |
| Metalöwdin | 1 | 0.031710 | 0.501463 | 0.032267 | 0.503212 |
| | 2 | 0.028989 | 0.492546 | 0.029836 | 0.495390 |
| | 3 | 0.028959 | 0.492444 | 0.029811 | 0.495307 |
| | 4 | 0.031721 | 0.501499 | 0.032280 | 0.503254 |
| NAO | 1 | 0.030891 | 0.498845 | 0.030997 | 0.499188 |
| | 2 | 0.028415 | 0.490581 | 0.028772 | 0.491806 |
| | 3 | 0.028385 | 0.490477 | 0.028747 | 0.491721 |
| | 4 | 0.030903 | 0.498886 | 0.031011 | 0.499233 |
| IAO | 1 | 0.032970 | 0.505386 | 0.032995 | 0.505462 |
| | 2 | 0.030183 | 0.496538 | 0.030547 | 0.497731 |
| | 3 | 0.030151 | 0.496432 | 0.030522 | 0.497647 |
| | 4 | 0.032983 | 0.505426 | 0.033009 | 0.505505 |

**Table A.13**: Aromaticity indices (MCI and $I_{ring}$) for each ring of the alcohol inner product substituent structure, computed using different population analysis partitions.

| Partition | Ring | MCI | $MCI^{1/2}$ | $I_{ring}$ | $I_{ring}{}^{1/2}$ |
|---|---|---|---|---|---|
| Mulliken | 1 | 0.460724 | 0.856423 | 0.233413 | 0.747524 |
| | 2 | 0.586617 | 0.898816 | -0.017855 | -0.447048 |
| | 3 | 1.625517 | 1.129140 | 0.322339 | 0.753491 |
| | 4 | 0.721616 | 0.936831 | 0.247888 | 0.756574 |
| | 5 | 0.395778 | 0.830788 | 0.205894 | 0.729002 |
| Löwdin | 1 | 0.016660 | 0.440897 | 0.020079 | 0.457664 |
| | 2 | -0.000192 | -0.180533 | 0.002550 | 0.302914 |
| | 3 | 0.005730 | 0.275133 | -0.002832 | -0.230696 |
| | 4 | -0.000105 | -0.160116 | 0.002508 | 0.301896 |
| | 5 | 0.015758 | 0.436013 | 0.019851 | 0.456621 |
| Metalöwdin | 1 | 0.032165 | 0.502893 | 0.031713 | 0.501473 |
| | 2 | 0.002877 | 0.310307 | 0.003230 | 0.317575 |
| | 3 | 0.001021 | 0.178771 | 0.000787 | 0.167499 |
| | 4 | 0.002714 | 0.306704 | 0.003057 | 0.314094 |
| | 5 | 0.030848 | 0.498706 | 0.031242 | 0.499976 |
| NAO | 1 | 0.032075 | 0.502612 | 0.031043 | 0.499337 |
| | 2 | 0.002215 | 0.294485 | 0.002203 | 0.294183 |
| | 3 | 0.001181 | 0.185369 | 0.000649 | 0.159637 |
| | 4 | 0.002106 | 0.291540 | 0.002089 | 0.291061 |
| | 5 | 0.030495 | 0.497560 | 0.030345 | 0.497069 |
| IAO | 1 | 0.033772 | 0.507821 | 0.032329 | 0.503407 |
| | 2 | 0.003077 | 0.314505 | 0.003213 | 0.317226 |
| | 3 | 0.000913 | 0.173847 | 0.000737 | 0.164782 |
| | 4 | 0.002943 | 0.311707 | 0.003046 | 0.313861 |
| | 5 | 0.032486 | 0.503893 | 0.031889 | 0.502028 |

**Table A.14**: Aromaticity indices (MCI and $I_{ring}$) for each ring of the alcohol outter product substituent structure, computed using different population analysis partitions.

| Partition | Ring | MCI | $MCI^{1/2}$ | $I_{ring}$ | $I_{ring}{}^{1/2}$ |
|---|---|---|---|---|---|
| Mulliken | 1 | 0.107445 | 0.640085 | 0.082561 | 0.607233 |
| | 2 | 0.542872 | 0.884992 | 0.269071 | 0.769083 |
| | 3 | 0.280244 | 0.727585 | 0.147649 | 0.619880 |
| | 4 | 0.598709 | 0.902492 | 0.299436 | 0.785707 |
| | 5 | -0.131035 | -0.666005 | 0.091708 | 0.620128 |
| Löwdin | 1 | 0.014855 | 0.430896 | 0.019439 | 0.454712 |
| | 2 | 0.000133 | 0.167900 | 0.002833 | 0.309360 |
| | 3 | 0.006478 | 0.283701 | -0.003311 | -0.239879 |
| | 4 | 0.000172 | 0.176738 | 0.002845 | 0.309606 |
| | 5 | 0.015528 | 0.434734 | 0.019800 | 0.456388 |
| Metalöwdin | 1 | 0.029209 | 0.493291 | 0.030057 | 0.496123 |
| | 2 | 0.002672 | 0.305755 | 0.003134 | 0.315654 |
| | 3 | 0.001065 | 0.180641 | 0.000656 | 0.160028 |
| | 4 | 0.002670 | 0.305702 | 0.003134 | 0.315653 |
| | 5 | 0.030215 | 0.496644 | 0.030726 | 0.498313 |
| NAO | 1 | 0.029161 | 0.493130 | 0.029407 | 0.493957 |
| | 2 | 0.001963 | 0.287459 | 0.002143 | 0.292548 |
| | 3 | 0.001053 | 0.180148 | 0.000573 | 0.154740 |
| | 4 | 0.001957 | 0.287283 | 0.002140 | 0.292481 |
| | 5 | 0.030180 | 0.496529 | 0.030076 | 0.496186 |
| IAO | 1 | 0.030801 | 0.498556 | 0.030742 | 0.498362 |
| | 2 | 0.002883 | 0.310444 | 0.003116 | 0.315304 |
| | 3 | 0.000782 | 0.167248 | 0.000511 | 0.150329 |
| | 4 | 0.002887 | 0.310513 | 0.003120 | 0.315378 |
| | 5 | 0.031815 | 0.501796 | 0.031435 | 0.500591 |

**Table A.15**: Aromaticity indices (MCI and $I_{ring}$) for each ring of the -t-Bu reactant substituent structure, computed using different population analysis partitions.

| Partition | Ring | MCI | $MCI^{1/2}$ | $I_{ring}$ | $I_{ring}{}^{1/2}$ |
|---|---|---|---|---|---|
| Mulliken | 1 | 0.015972 | 0.437191 | 0.095460 | 0.625121 |
| | 2 | 1.627805 | 1.102352 | 0.155164 | 0.688903 |
| | 3 | 1.631387 | 1.102837 | 0.297334 | 0.784601 |
| | 4 | 0.014995 | 0.431708 | 0.517056 | 0.876411 |
| Löwdin | 1 | 0.016252 | 0.438713 | 0.019461 | 0.454814 |
| | 2 | 0.015332 | 0.433628 | 0.018846 | 0.451902 |
| | 3 | 0.015328 | 0.433609 | 0.018843 | 0.451888 |
| | 4 | 0.016258 | 0.438746 | 0.019466 | 0.454835 |
| Metalöwdin | 1 | 0.030904 | 0.498887 | 0.031289 | 0.500126 |
| | 2 | 0.030488 | 0.497538 | 0.031027 | 0.499284 |
| | 3 | 0.030482 | 0.497518 | 0.031022 | 0.499269 |
| | 4 | 0.030915 | 0.498923 | 0.031297 | 0.500152 |
| NAO | 1 | 0.029933 | 0.495711 | 0.029899 | 0.495599 |
| | 2 | 0.029526 | 0.494356 | 0.029710 | 0.494972 |
| | 3 | 0.029520 | 0.494336 | 0.029705 | 0.494956 |
| | 4 | 0.029944 | 0.495748 | 0.029907 | 0.495627 |
| IAO | 1 | 0.032199 | 0.502999 | 0.031997 | 0.502368 |
| | 2 | 0.031723 | 0.501505 | 0.031762 | 0.501628 |
| | 3 | 0.031716 | 0.501484 | 0.031757 | 0.501613 |
| | 4 | 0.032211 | 0.503037 | 0.032005 | 0.502394 |

**Table A.16**: Aromaticity indices (MCI and $I_{ring}$) for each ring of the -t-Bu inner product substituent structure, computed using different population analysis partitions.

| Partition | Ring | MCI | $MCI^{1/2}$ | $I_{ring}$ | $I_{ring}{}^{1/2}$ |
|---|---|---|---|---|---|
| Mulliken | 1 | 0.113549 | 0.647197 | -0.127050 | -0.661904 |
| | 2 | 2.131220 | 1.163391 | 0.332889 | 0.802527 |
| | 3 | 1.713083 | 1.144049 | 1.449913 | 1.097326 |
| | 4 | 2.131379 | 1.163408 | 1.851477 | 1.131107 |
| | 5 | 0.113561 | 0.647211 | -0.127050 | -0.661904 |
| Löwdin | 1 | 0.017282 | 0.444140 | 0.020165 | 0.458058 |
| | 2 | -0.000985 | -0.250441 | 0.002028 | 0.289345 |
| | 3 | 0.005157 | 0.267981 | -0.003175 | -0.237379 |
| | 4 | -0.000985 | -0.250440 | 0.002028 | 0.289345 |
| | 5 | 0.017282 | 0.444141 | 0.020165 | 0.458058 |
| Metalöwdin | 1 | 0.034565 | 0.510185 | 0.033382 | 0.506644 |
| | 2 | 0.002315 | 0.297103 | 0.002807 | 0.308788 |
| | 3 | 0.000900 | 0.173205 | 0.000736 | 0.164726 |
| | 4 | 0.002315 | 0.297102 | 0.002807 | 0.308788 |
| | 5 | 0.034565 | 0.510185 | 0.033382 | 0.506645 |
| NAO | 1 | 0.034112 | 0.508841 | 0.032385 | 0.503581 |
| | 2 | 0.001526 | 0.273350 | 0.001665 | 0.278146 |
| | 3 | 0.000721 | 0.163875 | 0.000442 | 0.145018 |
| | 4 | 0.001526 | 0.273349 | 0.001665 | 0.278145 |
| | 5 | 0.034112 | 0.508841 | 0.032385 | 0.503581 |
| IAO | 1 | 0.036408 | 0.515514 | 0.034221 | 0.509165 |
| | 2 | 0.002497 | 0.301640 | 0.002802 | 0.308663 |
| | 3 | 0.000692 | 0.162220 | 0.000615 | 0.157499 |
| | 4 | 0.002497 | 0.301639 | 0.002802 | 0.308663 |
| | 5 | 0.036408 | 0.515514 | 0.034221 | 0.509165 |

**Table A.17**: Aromaticity indices (MCI and $I_{ring}$) for each ring of the -t-Bu outter product substituent structure, computed using different population analysis partitions.

| Partition | Ring | MCI | $MCI^{1/2}$ | $I_{ring}$ | $I_{ring}^{1/2}$ |
|---|---|---|---|---|---|
| Mulliken | 1 | 0.269900 | 0.769557 | 0.051330 | 0.552171 |
| | 2 | 0.522793 | 0.878347 | 0.129432 | 0.664367 |
| | 3 | 0.947525 | 0.986615 | 0.348987 | 0.768604 |
| | 4 | 0.523189 | 0.878480 | 0.110779 | 0.644008 |
| | 5 | 0.269735 | 0.769463 | 0.051007 | 0.551476 |
| Löwdin | 1 | 0.015235 | 0.433080 | 0.019208 | 0.453625 |
| | 2 | 0.000040 | 0.131693 | 0.002837 | 0.309437 |
| | 3 | 0.006340 | 0.282178 | -0.003403 | -0.241531 |
| | 4 | 0.000040 | 0.131690 | 0.002837 | 0.309438 |
| | 5 | 0.015235 | 0.433079 | 0.019208 | 0.453624 |
| Metalöwdin | 1 | 0.031259 | 0.500028 | 0.031223 | 0.499914 |
| | 2 | 0.002679 | 0.305903 | 0.003138 | 0.315736 |
| | 3 | 0.001003 | 0.177972 | 0.000594 | 0.156104 |
| | 4 | 0.002679 | 0.305902 | 0.003138 | 0.315736 |
| | 5 | 0.031258 | 0.500026 | 0.031223 | 0.499912 |
| NAO | 1 | 0.030702 | 0.498235 | 0.030406 | 0.497269 |
| | 2 | 0.001971 | 0.287689 | 0.002149 | 0.292708 |
| | 3 | 0.001001 | 0.177868 | 0.000519 | 0.150907 |
| | 4 | 0.001971 | 0.287688 | 0.002149 | 0.292709 |
| | 5 | 0.030702 | 0.498233 | 0.030405 | 0.497267 |
| IAO | 1 | 0.032824 | 0.504938 | 0.031894 | 0.502045 |
| | 2 | 0.002890 | 0.310574 | 0.003120 | 0.315375 |
| | 3 | 0.000715 | 0.163537 | 0.000442 | 0.145003 |
| | 4 | 0.002890 | 0.310574 | 0.003120 | 0.315376 |
| | 5 | 0.032823 | 0.504936 | 0.031894 | 0.502043 |